Regulation of stress-induced sleep perturbations by dorsal raphe VGLUT3 neurons in male mice

Fiona Henderson, Sylvie Dumas, Giuseppe Gangarossa, Véronique Bernard, Marine Pujol, Odile Poirel, Nicolas Pietrancosta, Salah El Mestikawy, Stéphanie Daumas, Véronique Fabre

Cell Reports

Regulation of stress-induced sleep perturbations by dorsal raphe VGLUT3 neurons in male mice

Graphical abstract

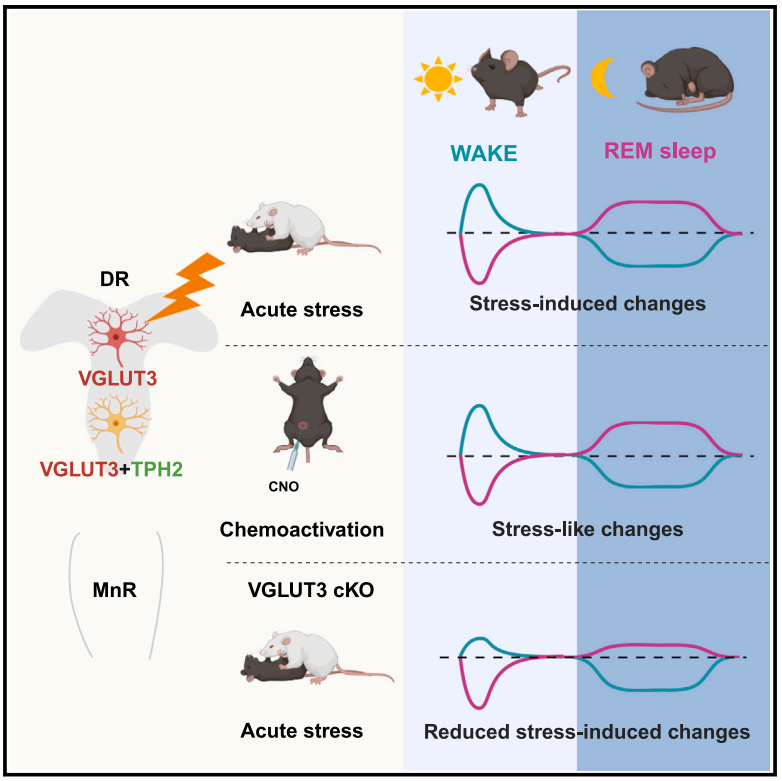

Highlights

- VGLUT3 expression identifies subsets of 5-HT and non-5-HT DR neurons activated by acute stress
- Selective activation of VGLUT3-expressing neurons in the DR modulates wake and REMS
- Reduced VGLUT3 expression in the DR attenuates stress-induced sleep perturbations
- VGLUT3 expression in 5-HT neurons exerts minimal influence on sleep

Authors

Fiona Henderson, Sylvie Dumas, Giuseppe Gangarossa, ..., Salah El Mestikawy, Stéphanie Daumas, Véronique Fabre

Correspondence

stephanie.daumas@sorbonne-universite.fr (S.D.), veronique.fabre@inserm.fr (V.F.)

In brief

Psychological stressors can induce maladaptive disruptions in sleep patterns. Henderson et al. show that neurons expressing VGLUT3 in the dorsal raphe nucleus (DR) are involved in the stress response and contribute to the circuit mechanisms mediating the effects of acute stress on sleep.

Henderson et al., 2024, Cell Reports *43*, 114411
July 23, 2024
https://doi.org/10.1016/j.celrep.2024.114411

CellPress

Cell Reports

CellPress
OPEN ACCESS

Report

Regulation of stress-induced sleep perturbations by dorsal raphe VGLUT3 neurons in male mice

Fiona Henderson,[1] Sylvie Dumas,[2] Giuseppe Gangarossa,[3,4] Véronique Bernard,[1] Marine Pujol,[1] Odile Poirel,[1] Nicolas Pietrancosta,[1,5] Salah El Mestikawy,[1,6] Stéphanie Daumas,[1,7,*] and Véronique Fabre[1,7,8,*]

[1]Sorbonne Université, CNRS UMR 8246, INSERM U1130 - Neuroscience Paris Seine - Institut de Biologie Paris Seine (NPS - IBPS), 75005 Paris, France
[2]Oramacell, 75006 Paris, France
[3]Université Paris Cité, CNRS, Unité de Biologie Fonctionnelle et Adaptative, 75013 Paris, France
[4]Institut Universitaire de France (IUF), Paris, France
[5]Sorbonne Université, CNRS UMR 7203, Laboratoire des BioMolécules, 75005 Paris, France
[6]Department of Psychiatry, Douglas Mental Health University Institute, McGill University, Montréal, QC H4H 1R3, Canada
[7]Senior author
[8]Lead contact
*Correspondence: stephanie.daumas@sorbonne-universite.fr (S.D.), veronique.fabre@inserm.fr (V.F.)
https://doi.org/10.1016/j.celrep.2024.114411

SUMMARY

Exposure to stressors has profound effects on sleep that have been linked to serotonin (5-HT) neurons of the dorsal raphe nucleus (DR). However, the DR also comprises glutamatergic neurons expressing vesicular glutamate transporter type 3 (DR^{VGLUT3}), leading us to examine their role. Cell-type-specific tracing revealed that DR^{VGLUT3} neurons project to brain areas regulating arousal and stress. We found that chemogenetic activation of DR^{VGLUT3} neurons mimics stress-induced sleep perturbations. Furthermore, deleting VGLUT3 in the DR attenuated stress-induced sleep perturbations, especially after social defeat stress. In the DR, VGLUT3 is found in subsets of 5-HT and non-5-HT neurons. We observed that both populations are activated by acute stress, including those projecting to the ventral tegmental area. However, deleting VGLUT3 in 5-HT neurons minimally affected sleep regulation. These findings suggest that VGLUT3 expression in the DR drives stress-induced sleep perturbations, possibly involving non-5-HT DR^{VGLUT3} neurons.

INTRODUCTION

Acute stress leads to a transient and sustained increase in wake to ensure proper adaptive behaviors. Subsequently, it produces a delayed increase in sleep during the recovery period.[1,2] Among other structures, the dorsal raphe nucleus (DR) is involved in the stress response and stress-related psychiatric disorders, with a key role assigned to serotonin (5-HT) neurons.[3,4] Acute stress exposure produces a sustained release of 5-HT within DR-projecting brain areas,[5–8] which contributes to the delayed effects of stress on rapid eye movement sleep (REMS).[5,9] Accordingly, constitutive deletion of 5-HT-related genes has been associated with a blunted increase in REMS after exposure to acute restraint stress (RS).[1,10] However, these seminal studies have manipulated the 5-HT system without considering its cellular and neurochemical heterogeneity.[11,12] Recent studies have revealed the great diversity of 5-HT DR ($DR^{5\text{-}HT}$) neurons in terms of cell types,[13–15] connectivity,[16,17] and/or electrophysiological properties.[18–20] In addition to 5-HT neurons, the DR also harbors GABA, dopamine (DA), and glutamate neurons.[21] Recently, considerable efforts have been dedicated to understanding the role of different subsets of DR neurons, with notable examples linked to stress and emotional behaviors.[17,22] For instance, a subset of $DR^{5\text{-}HT}$ neurons that target the ventral tegmental area (VTA) influences susceptibility to social stress.[23] DA and GABA neurons of the DR have additionally been implicated in stress responses[24,25] and arousal.[25,26] Together, these studies suggest a model in which stress engages distinct DR neuronal populations to promote adaptive responses.

A neuronal population of the DR that has received less attention consists of neurons expressing the vesicular glutamate transporter type 3 (VGLUT3), conferring these neurons the ability to signal through glutamate.[27–30] Interestingly, VGLUT3 is also present in a subset of $DR^{5\text{-}HT}$ neurons, enabling glutamate co-transmission[12] and enhancing 5-HT vesicular filing though a process known as vesicular synergy.[31–33] VGLUT3 neurons of the DR (DR^{VGLUT3}) are implicated in motivated behaviors,[30,34–37] feeding,[38,39] and neuropathic pain.[40] However, it is unknown whether DR^{VGLUT3} neurons play a role in the regulation of sleep. Here, we examined the contribution of DR^{VGLUT3} neurons in the stress response and stress-induced sleep perturbations by using conditional gene deletion and chemogenetics coupled with polygraphic sleep recordings. Additionally, potential targets were identified through conditional viral tracing and c-Fos immunolabeling.

RESULTS

Anatomical organization of DR^{VGLUT3} neurons

In the raphe, expression of VGLUT3 defines restricted subsets of neurons, as revealed by the seminal study conducted by Hioki in the rat DR.[41] Co-expression profiles in 5-HT neurons vary across raphe nuclei, with the median raphe nucleus (MnR) showing higher levels of segregation between 5-HT and VGLUT3 neurons.[12,42] We thus systematically mapped the expression pattern of VGLUT3 mRNA in relation to 5-HT neurons in the anterior raphe nuclei by dual fluorescence *in situ* hybridization (FISH; Figures 1A, S1A, and S1B). Tryptophan hydroxylase type 2 (TPH2) mRNA was used as a 5-HT marker. We found that VGLUT3 neurons co-expressing TPH2 mRNA were mostly observed in the caudal (DRc) and ventral (DRv) parts of the DR (Figure 1B). Consistent with previous findings,[41,42] single-labeled VGLUT3 mRNA neurons were more prevalent in B9, MnR, the interpeduncular nucleus (IP), and the dorsal part of the DR, while the lateral wings of the DR contained few VGLUT3 mRNA-expressing neurons (Figures 1A and 1B).

Next, we generated a VGLUT3^{Cre} mouse line (Figure 1C for visualizing Cre expression in DR^{VGLUT3} neurons) to map DR^{VGLUT3} projections by micro-injecting an adeno-associated virus (AAV) enabling Cre-dependent expression of the fluorescent protein tdTomato into their DR (AAV-Flex-tdTomato, Figures 1D, 1E, and S1C). DR^{VGLUT3} neurons heavily projected to the diagonal band nucleus/magnocellular nucleus (NDB/MA), the cortex, the basolateral (BLA) and cortical amygdala, the submedius thalamic nucleus, the anterior pretectal nucleus, and the VTA (Figure 1F; Table S1). Projections were dense in the prelimbic cortex (PL), the nucleus accumbens (NAc), the locus coeruleus (LC), and the parabrachial nucleus (PB) (Figure 1F; Table S1). This projection pattern closely resembles the distribution of DR$^{5\text{-}HT}$ terminals within the mouse brain.[16] Additional immunostaining with 5-HT (Figures 1G and S1D) showed that the majority of DR^{VGLUT3}-tdTomato fibers were 5-HT positive in the PL and NDB/MA, as previously found in the cortex.[17] Many DR^{VGLUT3}-tdTomato fibers were 5-HT negative in the amygdala, VTA, PB, and LC despite dense 5-HT labeling, consistent with previous data in the amygdala[17,29] and VTA.[16,35] While being involved in several other functions, these structures regulate the stress responses[44] and/or promote wake,[45] suggesting that DR^{VGLUT3} neurons may contribute to stress-induced arousal.

Chemoactivation of DR^{VGLUT3} neurons modulates vigilance states

To reveal which downstream target is functionally connected to DR^{VGLUT3} neurons, we mapped c-Fos expression, a *bona fide* marker of molecular neuronal activity, after selective activation of DR^{VGLUT3} neurons with the excitatory hM3(Gq) designer receptors exclusively activated by designer drugs (DREADDs; Figures 2A and 2B). Indeed, c-Fos expression, assessed 90 min after administration of the DREADD ligand clozapine N-oxide (CNO; 1 mg/kg, intraperitoneally) at zeitgeber time (ZT) 3, was significantly increased in the DR of mice expressing hM3(Gq) (VGLUT3-Gq) compared to mice expressing mCherry (VGLUT3-mCh; Figures 2C and 2D). Further analysis revealed increased c-Fos expression in the NAc, VTA, and PB of VGLUT3-Gq compared to VGLUT3-mCh mice (Figures 2E and 2F), indicating functional connectivity of DR^{VGLUT3} neurons to arousal-driving brain regions.[46–48] Accordingly, we analyzed vigilance states after CNO (1 mg/kg) or saline injections to VGLUT3-Gq and VGLUT3-mCh mice at ZT3 (Figures 2G and S2A). Across the first 3 h after injection in the light-inactive period (ZT3–ZT6), CNO increased wake amounts compared with saline-treated animals in VGLUT3-Gq mice (Figure 2H). In parallel, REMS amounts were decreased in CNO-treated VGLUT3-Gq mice compared with respective controls. This decrease was accounted for by a decrease in the number of state bouts (Table S2). Delayed effects included increased REMS amounts, at the expense of wake, during the first 6 h of the following dark-inactive period in CNO- compared with saline-injected VGLUT3-Gq mice due to a higher number of state bouts (Figure 2H; Table S2). Predominant targeting of the DR is further shown by mapping the injection sites in VGLUT3-Gq mice (Figures S2C and S2D). In a few mice, a sparse number of transduced cells was also observed in the upper part of the MnR.

Given the involvement of the DR in thermoregulation,[50] we monitored skin and brown adipose tissue temperatures in VGLUT3-mCh and VGLUT3-Gq mice before and 3 h after CNO injection (Figure S2B). No significant modifications were observed, suggesting that the sleep changes induced by chemoactivation are unlikely to be associated with changes in energy expenditure.

DR^{VGLUT3} neurons are involved in the stress response

Chemoactivation of DR^{VGLUT3} neurons at ZT3 mimics sleep-wake effects observed after acute social defeat (SD) stress during the light-inactive period.[2,51] Consequently, we investigated the role of DR^{VGLUT3} neurons in mediating SD-induced sleep perturbations.

SD (25 min session ending at ZT3) increased the activity of DR^{VGLUT3} neurons (Figures 3A–3C), including both 5-HT and non-5-HT types (Figures 3D and 3E). The VTA receives dense innervation from DR^{VGLUT3} neurons and is a key node for mediating SD-induced sleep changes.[52] We therefore evaluated whether DR^{VGLUT3} neurons projecting to the VTA were activated by SD. To identify VTA-projecting DR^{VGLUT3} neurons, a retrograde AAV enabling the conditional expression of the green fluorescence protein (GFP) was injected into the VTA of VGLUT3^{Cre} mice (Figures 3F and 3G). Consistent with earlier findings,[35,41,53] we identified GFP neurons in the DRv and the ventral part of the DRc, the IP, and the MnR. VTA-projecting DR^{VGLUT3} neurons, mainly those that are non-5-HT, were activated by SD (Figures 3H–3J).

Next, we investigated the impact on sleep of VGLUT3 deletion mediated by AAV-Cre-EGFP injection in the DR of VGLUT3$^{lox/lox}$ mice (+Cre; Figure 3K). VGLUT3 mRNA expression was significantly reduced in the DR (Figures 3L and 3M) and the MnR (52% ± 9%; data not shown) of +Cre mice compared with −Cre controls, while TPH2 mRNA expression remained unaffected (Figure 3L). Then, we examined the impact of VGLUT3 deletion on sleep-wake states. At baseline, +Cre mice spent more time in non-REMS (NREMS) and less time in wake during the dark-active period compared with −Cre mice (Figure S3A; Table S3). The consequences of SD were evaluated in +Cre

CellPress
OPEN ACCESS

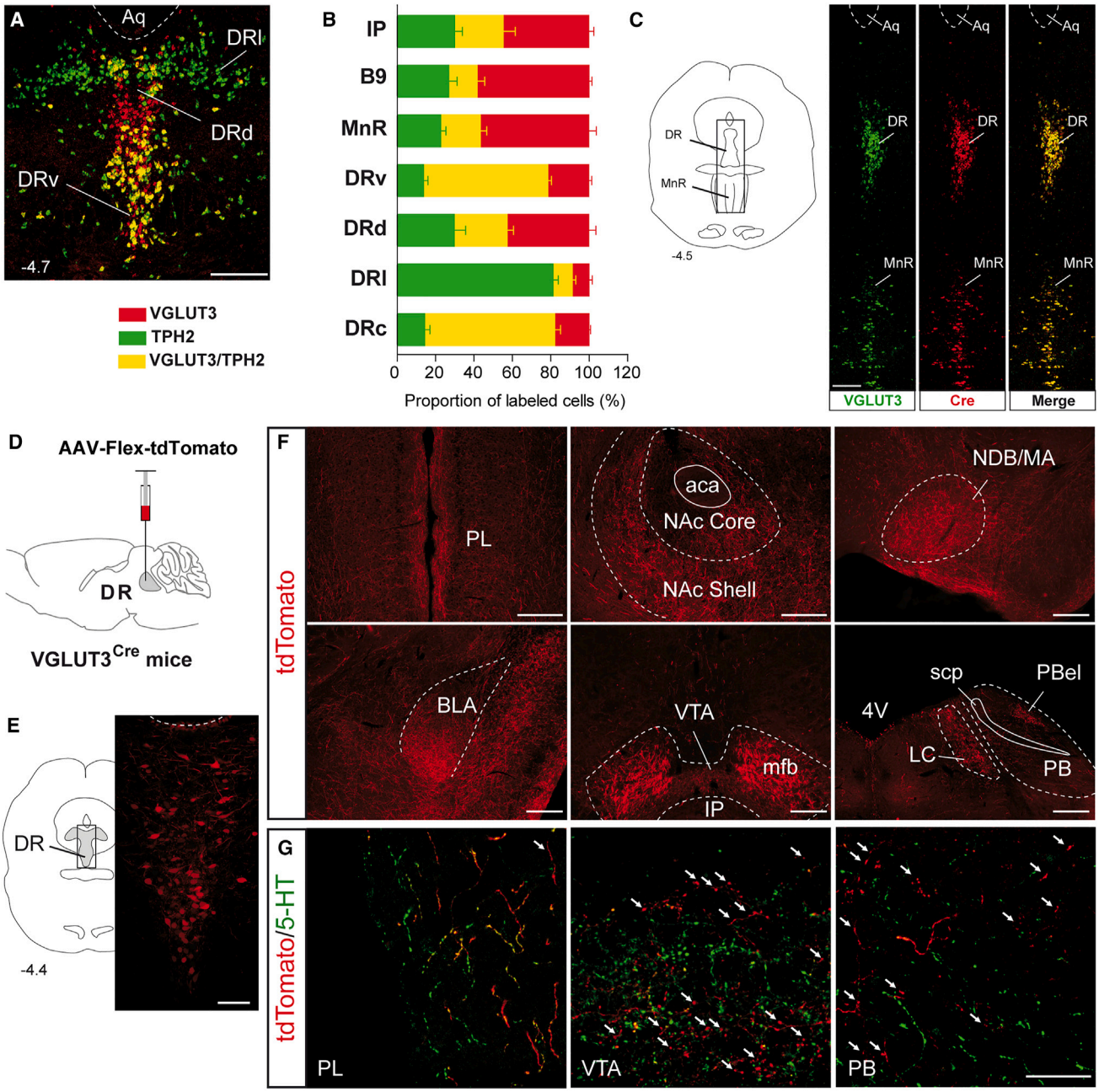

Figure 1. Distribution and projections of DR^{VGLUT3} neurons

(A and B) Representative image (A) and quantification (B) of cells expressing VGLUT3, TPH2, and both mRNAs in mouse anterior raphe nuclei. Data (mean ± SEM) are expressed as a percentage over the total number of VGLUT3-cells (n = 3).

(C) Distribution of cells expressing VGLUT3, Cre, and both (merged image) mRNAs in the anterior raphe nuclei of VGLUT3^{Cre} mice.

(D) Schematic of virus injection.

(E) Image showing tdTomato (red) expression in the DR of VGLUT3^{Cre} mice.

(F) Anterolabeled terminals (red) are present in the PL, NAc shell, NDB/MA, BLA, VTA, LC, and PB nuclei.

(G) 5-HT immunolabeling (green), tdTomato anterolabeled (red), and double-labeled (yellow) terminals in the PL, VTA, and PB of VGLUT3^{Cre} mice. White arrows: single tdTomato anterolabeled terminals. Coronal sections were adapted from the stereotaxic atlas.[43] Distance from bregma is indicated in mm.[43]

Scale bars: 250 μm in (A), 150 μm in (C), 100 μm in (E), 300 μm in (F), and 25 μm in (G).

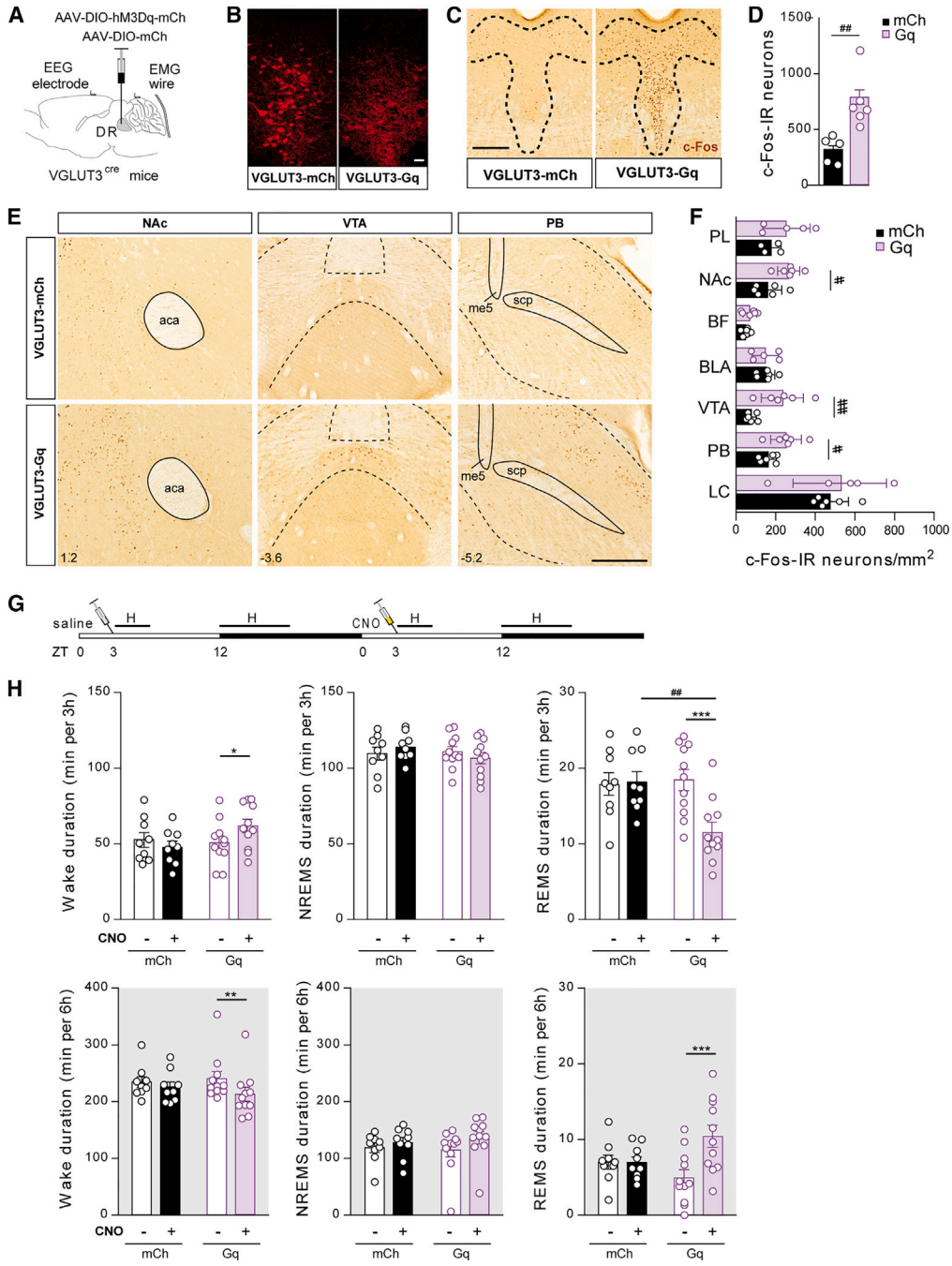

Figure 2. Chemogenetic activation of DR^{VGLUT3} neurons modulates wake and REMS

(A) Schematic of virus injection and electrode implantation.

(B) Representative images showing mCherry (red) expression in the DR of VGLUT3-Gq and VGLUT3-mCh mice.

(C and D) Representative images (C) and quantification (D) of c-Fos-immunoreactive (C-Fos-IR) cells in the DR of VGLUT3-Gq (Gq; $n = 6$) and VGLUT3-mCh (mCh; $n = 5$) mice after CNO injection.

(E and F) Representative images (E) and quantification (F) of c-Fos-IR cells in brain areas of interest of VGLUT3-Gq (Gq; $n = 6$) and VGLUT3-mCh (mCh; $n = 5$) mice after CNO injection. Distance from bregma is indicated in mm.[49]

(G) Experimental design. Letters above the horizontal bars represent the time window analyzed in (H).

(H) State amounts during the first 3 h (top) and the first 6 h of the dark period (bottom) following saline (−) or CNO (+) injections at ZT3 in hM3Dq-expressing (Gq; $n = 11$) and control (mCh; $n = 9$) mice.

Scale bars: 50 μm in (B), 250 μm in (C), and 300 μm in (E). Data represent the mean ± SEM. Post hoc comparisons: $^{*}p < 0.05$, $^{**}p < 0.01$, and $^{***}p < 0.001$ for CNO effects; $^{\#}p < 0.05$ and $^{\#\#}p < 0.01$ for group effects. See also Table S6.

and −Cre mice (Figures 3N and S3B). In control mice, SD elicited an immediate and robust increase in wake amounts and a concomitant decrease in NREMS and REMS amounts (ZT3–ZT6 of the light-inactive period; Figure 3O). These changes were mainly accounted for by changes in bout mean duration (Table S4). During the subsequent dark-active period (ZT12–ZT0), −Cre mice exhibited increased REMS amounts following SD resulting from an increased number of bouts (Figure 3O; Table S4). Strikingly, a clear phenotype emerged after SD. Short-term wake enhancement elicited by SD was attenuated in +Cre mice (Figure 3O). Moreover, +Cre mice lacked the REMS sleep rebound elicited by SD in the following dark-active period (Figure 3O). This sleep phenotype, likely linked to DR neurons, suggests a role for VGLUT3 in both SD-mediated immediate wake promotion (at the expense of NREMS) and delayed REMS facilitation, although MnR involvement cannot be discounted.

RS is a common model used in rodents, engaging similar circuits as SD.[54] RS at the end of the light-inactive period enhances sleep during the subsequent dark-active period, primarily affecting REMS through the DR and the 5-HT system.[1,5,10,55] Consequently, we investigated DR^{VGLUT3} neuron activity in response to RS (Figure 4A), finding increased c-Fos expression (Figures 4B and 4C) in both 5-HT and non-5-HT DR^{VGLUT3} neurons (Figures 4D and 4E). We next tested the impact of RS on sleep and wake in mice with AAV-Cre-mediated deletion of VGLUT3 expression in the DR (Figure 4F). In −Cre mice, RS applied at the end of the light-inactive period produced an increase in sleep amounts throughout the following dark-active period (Figures 4G and S3C). Notably, REMS amounts were enhanced by ~2-fold as a result of an increase in both the number and mean duration of REMS bouts (Table S4). After RS, +Cre mice exhibited more REMS compared to the sham condition (Figure 4G). However, analysis of delta changes suggests that RS affected REMS differently across groups, with +Cre mice exhibiting a reduced REMS rebound (Figure 4G). In addition, +Cre mice exhibited more REMS compared to −Cre mice in the sham condition (Figure 4G). This could have been a consequence of the experimental paradigm, in which mice were gently woken up in the sham condition (see STAR Methods).

Psychological stressors trigger a rapid increase in body temperature through VGLUT3 neurons.[56,57] However, skin temperature measurements after SD and RS showed stress-induced hyperthermia in both −Cre and +Cre mice (Figure S4). This suggests that stress-induced sleep perturbations in +Cre mice occurred independently of the potentially confounding effects of body temperature.

VGLUT3 in 5-HT neurons has limited effects on vigilance states

Considering the key role of 5-HT neurons in sleep-wake regulation,[58] we investigated the impact of VGLUT3 in these neurons by generating mice lacking VGLUT3 in 5-HT neurons. Mice expressing Cre recombinase under the control of the serotonin transporter (SERT) promoter were crossed with $VGLUT3^{lox/lox}$ mice ($SERT^{VGLUT3.cKO}$, where cKO is conditional knockout) (Figure 5A). Validation confirmed specific Cre-mediated deletion of VGLUT3 in 5-HT neurons (Figures 5B and S5). In $SERT^{VGLUT3.cKO}$ mice, DR neurons expressed either TPH2 mRNA or VGLUT3 mRNA, but co-labeled neurons (as observed in control $SERT^{Cre}$ mice) were not detected. Next, sleep-wake patterns were analyzed in $SERT^{VGLUT3.cKO}$ mice and control ($VGLUT3^{lox/lox}$ and $SERT^{Cre}$) mice. VGLUT3 deletion in 5-HT neurons did not alter sleep-wake amounts at baseline (Figure S6; Table S3). Then, we assessed the consequences of chemoactivation of $DR^{5\text{-}HT}$ neurons with or without VGLUT3. AAV-DIO-hM3(Gq)-mCh or AAV-DIO-mCh was injected into the DR of $SERT^{Cre}$ (SERT-Gq and SERT-mCh) and $SERT^{VGLUT3.cKO}$ ($SERT^{VGLUT3.cKO}$-Gq and $SERT^{VGLUT3.cKO}$-mCh) mice (Figure 5A). Sleep-wake states were analyzed after administration of CNO or saline at ZT3 (Figure 5C). As reported by others,[59,60] we observed non-specific effects of CNO on REMS in SERT-mCh and $SERT^{VGLUT3.cKO}$-mCh mice (Figure 5D). However, the use of non-DREADD-expressing control groups has enabled comparisons with DREADD-expressing groups to identify the effects of chemoactivation of $DR^{5\text{-}HT}$ neurons. These off-target CNO effects were absent in $VGLUT3^{Cre}$ mice (Figure 2), possibly due to genetic background differences (see STAR Methods).

NREMS amounts increased in the 3 h post-CNO injection compared with saline injection in SERT-Gq mice, while REMS amounts decreased significantly compared to saline injection and with CNO-treated SERT-mCh mice (Figures 5D and S7A). These effects were due to the longer mean duration of NREMS bouts and fewer REMS bouts, respectively (Table S2). Similar immediate effects were observed in $SERT^{VGLUT3.cKO}$ mice after chemogenetic activation of $DR^{5\text{-}HT}$ neurons (Figure 5D, S7B, and S7C). During the first 6 h of the following dark-active period, CNO did not alter sleep-wake states in SERT-Gq mice (Figures 5D and S7A; Table S2). In $SERT^{VGLUT3.cKO}$-Gq mice, CNO induced a significant increase in wake amounts at the expense of NREMS compared with saline injection and had a limited impact on REMS amounts (Figures 5D and S7B). Thus, chemogenetic activation of $DR^{5\text{-}HT}$ neurons had a delayed impact on wake and NREMS in $SERT^{VGLUT3.cKO}$ mice only (Figure S7D). These results collectively suggest that VGLUT3 in 5-HT neurons plays a limited role in sleep regulation, a role that becomes apparent solely during the dark-active period following chemoactivation of $DR^{5\text{-}HT}$ neurons.

Because RS produces a delayed increase in REMS that depends on the DR serotonergic system,[55] $SERT^{VGLUT3.cKO}$ mice and their respective controls were subjected to RS (Figures 5E and S8; Table S5). After RS, $SERT^{VGLUT3.cKO}$ mice showed enhanced NREMS and REMS during the following dark-active period, as observed in control groups (Figure 5F). VGLUT3 is also expressed by subsets of GABA and cholinergic neurons.[33,61] We then evaluated the impact of RS in cKO mice lacking VGLUT3 in GABA or cholinergic neurons (Figures S9; Table S5). No differences were observed in the sleep-promoting effects of RS in cKO mice compared with their respective controls. Together, these results suggest that VGLUT3 expression in 5-HT, GABA, or cholinergic neurons does not contribute to sleep-wake regulation after RS.

Beyond their role in sleep regulation, VGLUT3 and 5-HT neurons have been identified as modulators of various functions, including anxiety and locomotion.[12,32,38] Consequently, we conducted behavioral assessments across our different models and

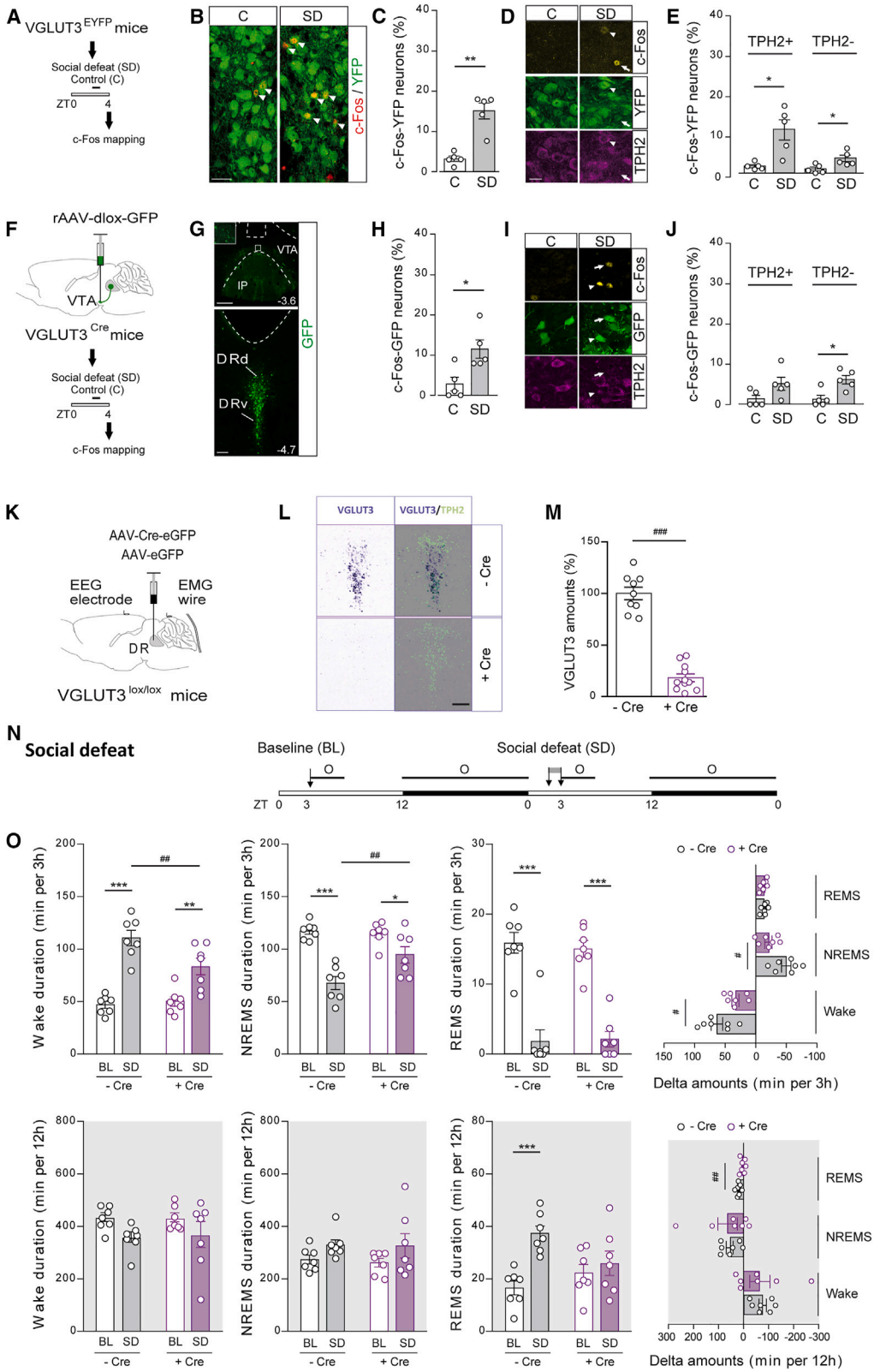

(legend on next page)

found that expression of VGLUT3 in DR or DR^{VGLUT3} neuron activation does not affect anxiety-like behaviors and locomotor activity (Figure S10).

DISCUSSION

Emotional events, especially stress, influence sleep-wake patterns. Our results suggest that DR^{VGLUT3} neurons are involved in mediating acute stress-induced sleep perturbations. Chemoactivation of DR^{VGLUT3} neurons promotes wakefulness by inhibiting REMS and subsequently promoting REMS, resembling stress-like effects. Further, reduced VGLUT3 expression mediated by AAV-Cre injection in the DR leads to compromised stress-induced sleep changes. Our data align with previous studies demonstrating VGLUT3 expression in subsets of 5-HT and non-5-HT neurons in the raphe nuclei.[41,42,62] Both types of DR^{VGLUT3} neurons are activated by stressors and project to PB, VTA, and NAc nuclei. Additional loss-of-function experiments suggest a minimal contribution of VGLUT3 in 5-HT neurons to sleep regulation. These findings suggest that non-5-HT VGLUT3 neurons, especially in the DR, modulate stress-induced sleep perturbations likely through mechanisms involving downstream structures that regulate emotional arousal and sleep recovery.

VGLUT3 in the DR modulates the stress response

In animals, arousal is an initial response to stress, and it seems to be regulated by VGLUT3 in the DR. Reduced VGLUT3 expression mediated by AAV-Cre injection in the DR was sufficient to attenuate arousal elicited by social stress. However, we could not assess this response after RS, as it did not induce arousal, likely due to differences in timing (ZT3 for SD versus ZT10.5 for RS) and/or duration of stressors (25 min for SD versus 90 min for RS), since both factors influence the sleep response to stress.[2,52,63,64] Results from social stress, coupled with reduced wake at baseline in mice lacking VGLUT3 in the DR and increased wake after activating DR^{VGLUT3} neurons, support their role in wake promotion. Previous studies also suggest that most DR neurons are wake promoting[25,26,45,58] and responsive to emotionally salient stimuli.[25,65–69] In agreement, we found that DR^{VGLUT3} neurons are activated by stress, including both 5-HT and non-5-HT DR^{VGLUT3} neurons. Together, these independent observations suggest that groups of DR neurons could promote arousal when a salient stimulus, such as facing a stressor, is perceived in the environment.

The initial stress response is followed by an increase in sleep during the subsequent dark-active period. Our results suggest that DR^{VGLUT3} neurons are involved in the delayed increase of sleep, particularly after exposure to social stress. Therefore, reduced VGLUT3 expression mediated by AAV-Cre injection in the DR dampens the delayed increase in REMS elicited by acute stress. This long-lasting impact of DR^{VGLUT3} neurons on sleep is also supported by our chemogenetic experiments showing that activation of DR^{VGLUT3} neurons produces a delayed increase in REMS amounts. In rodents, sleep enhancement is commonly observed in response to psychological stressors, SD,[51,52,64,70] or RS[10,63,71–73] and is not the sole consequence of the sleep loss associated with the stress procedure.[51,72] Strikingly, SD[51,52,64,70] or RS[10,63,71–73] trigger sleep enhancement independently of the stress schedule used. This highlights the crucial role of sleep in the stress response, supported by studies showing the beneficial effects of stress-induced sleep enhancement.[74] Conversely, sleep deprivation after social stress has negative effects on emotional behaviors.[52,75,76] It is therefore likely that the function of sleep after stress is to restore emotional reactivity, as proposed for REMS, which is thought to play an important role in processing emotional experiences[77–79] and potentiated fear responses.[80,81] DR^{VGLUT3} neurons may thus facilitate sleep-dependent adaptations to aversive experiences. Interestingly, constitutive VGLUT3 KO mice exhibit anxiety-like behavior,[32] innate fear,[82] and impaired fear memory.[83] Further research is needed to determine whether animals with VGLUT3 loss of

Figure 3. DR^{VGLUT3} neurons contribute to the response to SD stress

(A) Experimental design for c-Fos immunolabeling.

(B and C) Representative images (B) and quantification (C) of c-Fos immunolabeling in DR^{VGLUT3} neurons (c-Fos-YFP) after social defeat (SD) or in control (C) condition. White arrowheads: c-Fos/VGLUT3-positive neurons. Scale bar: 50 μm. $n = 5$.

(D and E) Representative images (D) and quantification (E) of c-Fos immunolabeling in DR^{VGLUT3} neurons (c-Fos-YFP) expressing (+) or not (−) TPH2 after SD or in control (C) condition. White arrowheads: triple c-Fos/TPH2/VGLUT3-positive neuron. White arrows: dual c-Fos/VGLUT3-positive neuron. Scale bar: 50 μm. $n = 5$.

(F) Experimental design for c-Fos immunolabeling in DR^{VGLUT3} neurons projecting to the VTA.

(G) Representative images showing rAAV-dlox-GFP injection site in the VTA (top, scale bar: 150 μm, the framed region corresponds to the inset in the left corner of the image) and GFP-expressing cells in the DR (bottom, scale bar: 100 μm) of VGLUT3^{Cre} mice.

(H) Quantification of c-Fos immunolabeling in VTA-projecting DR^{VGLUT3} neurons (c-Fos-GFP) after SD stress or in control (C) condition. $n = 5$.

(I and J) Representative images (I) and quantification (J) of c-Fos immunolabeling in VTA-projecting DR^{VGLUT3} neurons (c-Fos-GFP) expressing (+) or not (−) TPH2 after SD or in control (C) condition. White arrowheads: triple c-Fos/TPH2/VGLUT3-positive neuron. White arrows: dual c-Fos/VGLUT3-positive neuron. Scale bar: 50 μm. $n = 5$.

(K) Schematic of virus injection and electrode implantation.

(L) Representative image of the DR showing VGLUT3 (blue, bright field) and TPH2 (green, fluorescence) mRNAs in the DR of control (−Cre) and conditional knockout (+Cre) mice detected by dual ISH. Scale bar: 200 μm.

(M) Percentage of VGLUT3 mRNA expression in the DR of control (−Cre, black; $n = 9$) and conditional knockout (+Cre, purple, $n = 11$) mice.

(N) Experimental design. Letters above the horizontal bars represent the time windows analyzed in (O).

(O) State amounts during the first 3 h (top) and 12 h of the dark period (bottom) at baseline (BL) and after acute SD stress in control (−Cre, $n = 7$) and conditional knockout (+Cre, $n = 7$) mice. Delta amounts: difference between state amounts in SD and BL conditions.

Data represent the mean ± SEM. Post hoc comparisons: $^{*}p < 0.05$, $^{**}p < 0.01$, and $^{***}p < 0.001$ for stress effects; $^{\#}p < 0.05$, $^{\#\#}p < 0.01$, and $^{\#\#\#}p < 0.001$ for group effects.

See also Table S6.

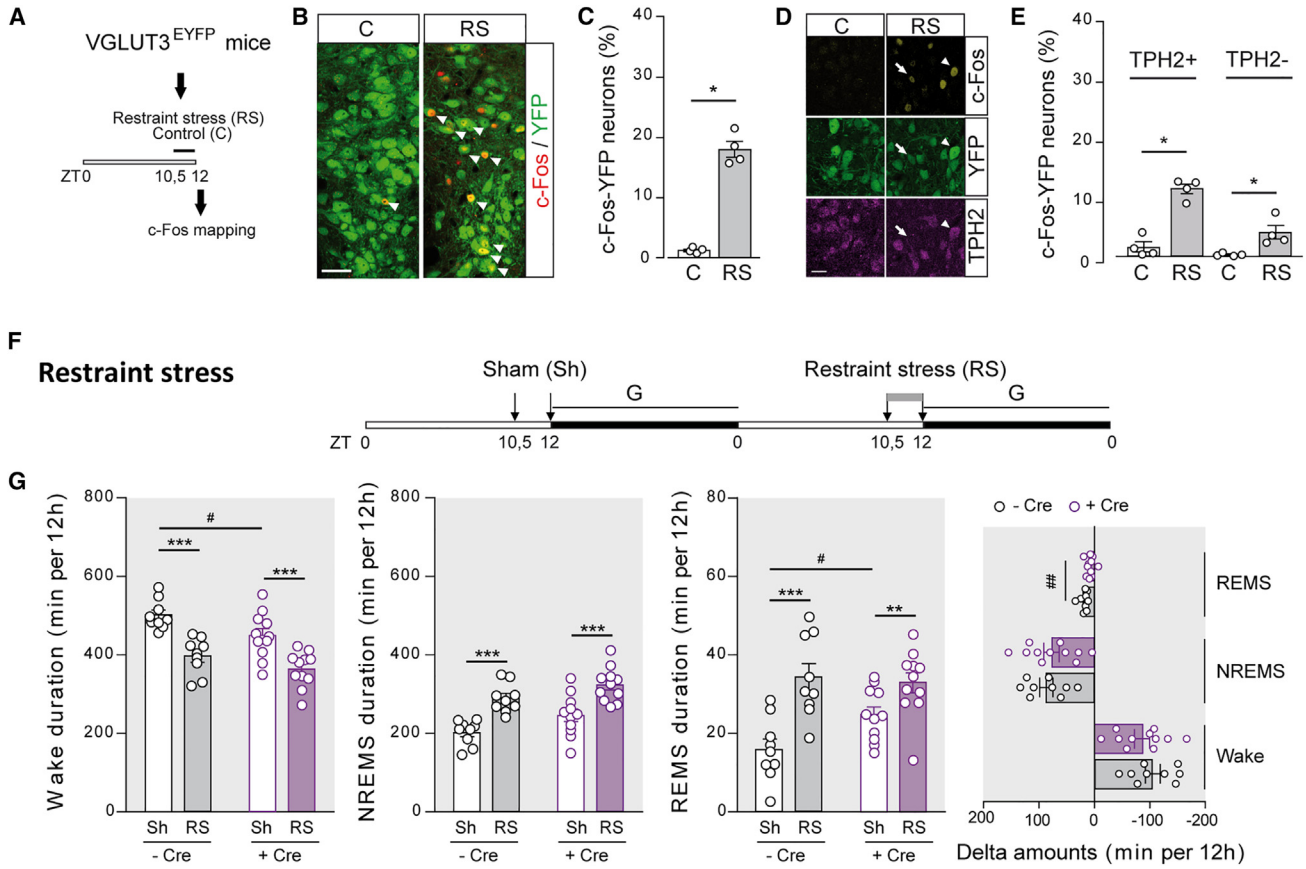

Figure 4. DR^{VGLUT3} neurons contribute to the response to RS

(A) Experimental design for c-Fos immunolabeling.

(B and C) Representative images (B) and quantification (C) of c-Fos immunolabeling in DR^{VGLUT3} neurons (c-Fos-YFP) after restraint stress (RS) or in control (C) condition. White arrowheads: c-Fos/VGLUT3-positive neurons. Scale bar: 50 μm. $n = 4$.

(D and E) Representative images (D) and quantification (E) of c-Fos immunolabeling in DR^{VGLUT3} neurons (c-Fos-YFP) expressing (+) or not (−) TPH2 after RS or in control (C) condition. White arrowheads: triple c-Fos/TPH2/VGLUT3-positive neuron. White arrows: dual c-Fos/VGLUT3-positive neuron. Scale bar: 50 μm. $n = 4$.

(F) Experimental design. Letters above the horizontal bars represent the time window analyzed in (G).

(G) State amounts during the first 12 h following sham (Sh) or acute RS in control (−Cre, $n = 9$) and conditional knockout (+Cre, $n = 11$) mice. Delta amounts: difference between state amounts in RS and Sh conditions.

Data represent the mean ± SEM. Post hoc comparisons: $^{*}p < 0.05$, $^{**}p < 0.01$, and $^{***}p < 0.001$ for stress effects; $^{\#}p < 0.05$ and $^{\#\#}p < 0.01$ for group effects. See also Table S6.

function in the DR are more susceptible to developing anxiety- and depression-like behaviors in response to stress and/or sleep disturbances.

Role of VGLUT3 expression in 5-HT neurons in the modulation of sleep-wake states

The DR contains distinct populations of neurons,[21,84] including non-5-HT and 5-HT neurons, with VGLUT3 expression observed in both types (Figure 1).[15,17,41] In 5-HT neurons, VGLUT3 enables glutamate co-release from 5-HT terminals, as shown in the VTA,[23,30,36] amygdala,[29] and olfactory bulb.[28] While a few studies have shown the involvement of glutamate co-release in reward,[30,36] little is known about the behavioral consequences of VGLUT3 expression in DR$^{5\text{-HT}}$ neurons. Given their role in sleep-wake regulation,[58] some effects of manipulating VGLUT3 neurons may involve DR$^{5\text{-HT}}$ neurons. To probe this hypothesis, we used mice with VGLUT3 deletion in SERT neurons. We found that chemoactivation of DR$^{5\text{-HT}}$ neurons had major effects on REMS that are independent from the presence of VGLUT3. This was further supported by the finding that deletion of VGLUT3 in 5-HT neurons does not impact sleep-wake amounts at baseline or after RS. From these experiments, we concluded that 5-HT neurons likely regulate sleep-wake states by signaling through 5-HT. Similarly, a prominent role for 5-HT over glutamate signaling has been reported in the amygdala during fear processing.[85] Independent of sleep regulation, the involvement of 5-HT-positive DR^{VGLUT3} neurons in the stress response is supported by their activation following acute stress and a recent study indicating that mutant mice lacking VGLUT3 in 5-HT neurons exhibit heightened active coping behavior in response to swim stress.[86]

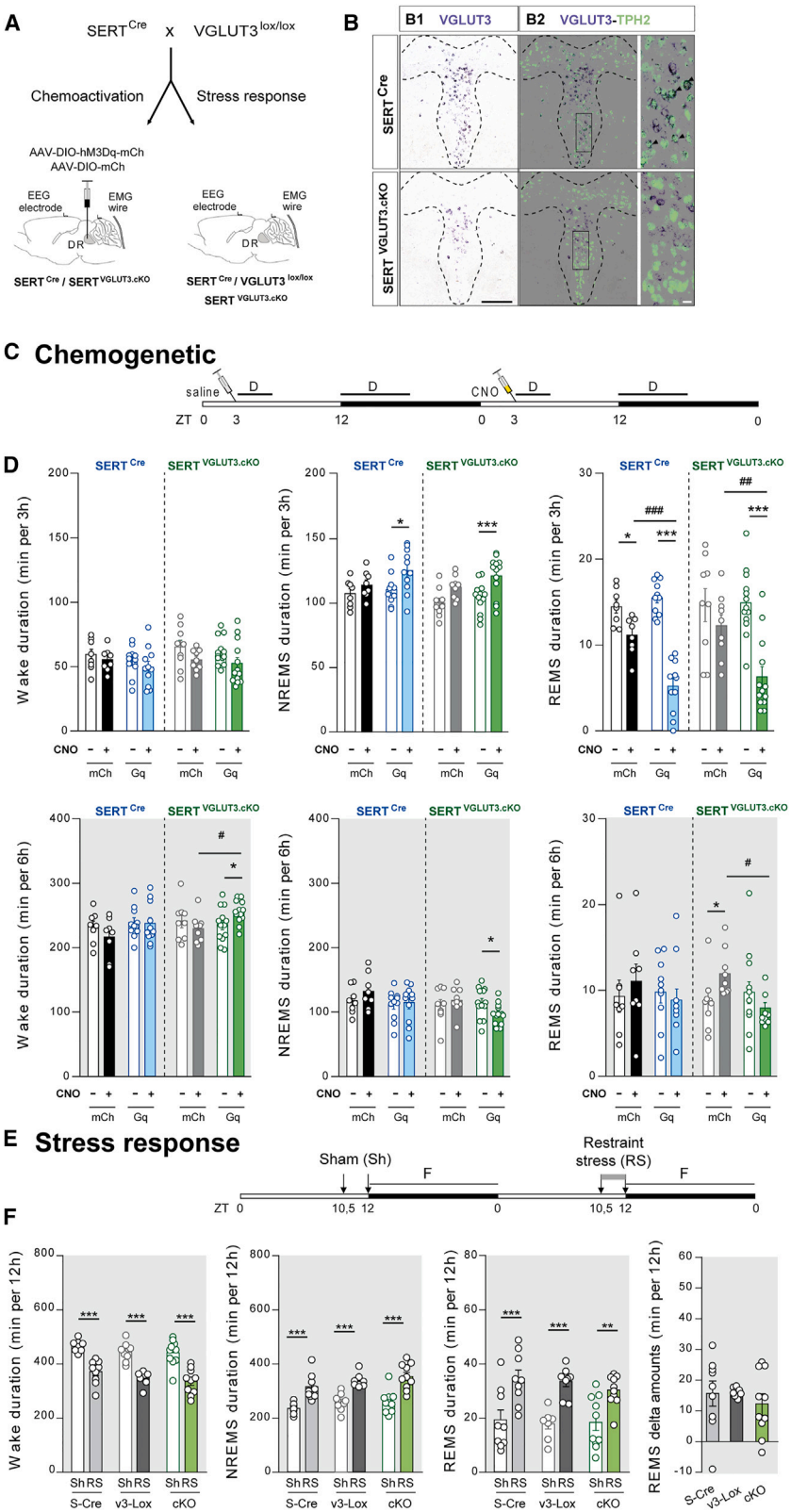

Figure 5. VGLUT3 expression in 5-HT neurons is not essential for sleep modulation

(A) Conditional knockout (SERT$^{VGLUT3.cKO}$) mice are generated by crossing SERT^{Cre} and VGLUT3$^{lox/lox}$ mice. Schematic of viral injection and electrode implantation strategies for assessing sleep response to chemoactivation of DR$^{5\text{-}HT}$ neurons or stress.

(B) Validation of VGLUT3 mRNA deletion in 5-HT neurons in SERT$^{VGLUT3.cKO}$ mice. VGLUT3 mRNA expression (blue, bright-field ISH, B1) and combined VGLUT3 (blue, bright-field ISH) and TPH2 (green, FISH) mRNA expression (B2) in the DR of control (SERT^{Cre}, top) and conditional knockout (SERT$^{VGLUT3.cKO}$, bottom) mice. Scale bar: 250 μm. Boxed areas in (B2) are magnified on the right. Double-labeled neurons (pointed at by a black arrowhead) are not observed in SERT$^{VGLUT3.cKO}$ mice. Scale bar: 25 μm.

(C) Experimental design. Letters above the horizontal bars represent the time windows analyzed in (D).

(D) State amounts during the first 3 h (top) or during the first 6 h of the dark period (bottom) following saline (−) or CNO (+) injections in (1) control (mCh) SERT^{Cre} (black, n = 8) and SERT$^{VGLUT3.cKO}$ (n = 9) mice and (2) hM3Dq-expressing (Gq) SERT^{Cre} (n = 11) and SERT$^{VGLUT3.cKO}$ (n = 13) mice. Data represent the mean ± SEM. Post hoc comparisons: $^{*}p < 0.05$ and $^{***}p < 0.001$ for CNO effects; $^{\#}p < 0.05$, $^{\#\#}p < 0.01$, and $^{\#\#\#}p < 0.001$ for group effects. See also Table S6.

(E) Experimental design. Letters above the horizontal bars represent the time window analyzed in (F).

(F) State amounts during the first 12 h following Sh or acute RS in SERT^{Cre} (S-Cre; n = 9), VGLUT3$^{lox/lox}$ (v3-Lox; n = 8), and SERT$^{VGLUT3.cKO}$ (cKO; n = 10) mice. Delta amounts: difference between REMS amounts in RS and Sh conditions. Data represent the mean ± SEM. Post hoc comparisons: $^{**}p < 0.01$ and $^{***}p < 0.001$ for stress effects. See also Table S6.

Our experiments suggest a role for non-5-HT DR^{VGLUT3} neurons in sleep regulation. Accordingly, wake-active non-5-HT neurons are distributed throughout the DR,[87] including the dorsal part, where many non-5-HT DR^{VGLUT3} neurons are found. However, expression of VGLUT3 in the DR is not reduced to the same extent in +Cre mice (−80%) and SERT$^{VGLUT3.cKO}$ mice (−50%, in agreement with results of dual FISH). This difference may explain why the two models differ in their stress responses. Additionally, AAV-Cre injection into the DR affects VGLUT3 expression not only in the DR (−80%) but also in the MnR (−50%). This suggests that the observed effects may also involve MnR neurons. However, these neurons are not activated by RS (Figure S11). While the influence of MnR neurons on sleep-wake patterns remains scarcely explored and cannot be discounted, they are implicated in emotional behaviors.[88,89]

We also observed that DR$^{5\text{-}HT}$ and DR^{VGLUT3} neurons can exert cell type-specific modulation on sleep-wake states. Using chemogenetics, we found that DR^{VGLUT3} neurons enhance wake amounts and subsequently promote REMS, whereas chemoactivation of DR$^{5\text{-}HT}$ neurons primarily promotes NREMS without delayed effects. The functional diversity within the DR is further supported by electrophysiological studies showing heterogeneous activity patterns of neurons based on their neurotransmitter released[18] or sleep-wake states.[87,90] In the MnR of anesthetized rats, non-5-HT VGLUT3 neurons exhibit more sustained responses to sensory stimuli compared to 5-HT neurons.[62] Heterogeneity is further revealed by optogenetic studies showing that inhibition of DR$^{5\text{-}HT}$ neurons or DR^{VGLUT3} neurons prior to the conditioning has an opposite impact on cocaine-induced place preference.[37] However, it is important to note that both populations can also have synergistic actions. Thus, we found that chemogenetic activation of DR$^{5\text{-}HT}$ neurons and/or DR^{VGLUT3} neurons decreased REMS amounts. Overall, our chemogenetic approaches suggest that DR$^{5\text{-}HT}$ and DR^{VGLUT3} neurons have complex and partially opposite roles in sleep regulation.

Downstream targets of DR^{VGLUT3} neurons involved in sleep regulation

Using conditional viral tracing, we observed DR^{VGLUT3} neuron terminals in multiple brain structures implicated in the regulation of sleep including the medial pre-frontal cortex, NAc, basal forebrain, BLA, VTA, PB, and LC.[47,91–95] By mapping c-Fos expression following chemoactivation of DR^{VGLUT3} neurons, we identified increased activity in the NAc, VTA, and PB. Elevated PB activity may mediate wakefulness elicited by DR^{VGLUT3} neurons, as local deletion of VGLUT2 reduces wake amounts in mice.[46,96] The VTA houses neuronal populations with opposite roles in sleep-wake regulation: dopaminergic and glutamatergic/nitrergic neurons promote wakefulness, while somatostatin/GABAergic neurons induce sleep.[47,97] Notably, VTA somatostatin/GABAergic neurons facilitate sleep recovery after social stress,[52] suggesting that they may be key targets of DR^{VGLUT3} neurons. Our findings also suggest that DR^{VGLUT3} neurons projecting to the VTA, particularly non-5-HT ones, are activated by social stress, further implicating them in stress responses. In addition, VTA neurons promote wake through projections to the NAc, which is functionally targeted by DR^{VGLUT3} neurons. In the NAc, neurons that express the adenosine $A2_A$ receptor or the DA D1 receptor promote NREMS or behavioral arousal, respectively.[48,91] Thus, the PB, VTA, and NAc could represent the potential mediators of a network involving DR^{VGLUT3} neurons. This hypothesis is coherent with the presence of many 5-HT-negative terminals originating from DR^{VGLUT3} neurons and the role we propose for non-5-HT DR^{VGLUT3} neurons in driving stress-induced sleep changes.

Limitations of the study

Our findings suggest a role for non-5-HT DR^{VGLUT3} neurons in stress-induced sleep perturbations. However, we inhibited VGLUT3 expression in both 5-HT and non-5-HT neurons, as well as solely in 5-HT neurons. Targeted manipulation of non-5-HT DR^{VGLUT3} neurons through intersectional strategy is warranted to confirm their role in sleep-wake regulation. Additionally, it is crucial to assess the impact of our viral strategy on the MnR, which contains a high number of non-5-HT VGLUT3 neurons. Pathway-specific genetic and neuronal manipulations can help differentiate the contributions of the DR versus the MnR. Furthermore, the precise mechanisms underlying stress-induced sleep perturbations by VGLUT3 neurons remain incompletely understood. To gain further insights, manipulating VGLUT3 terminals in functionally connected brain regions like the VTA could provide valuable information.

STAR★METHODS

Detailed methods are provided in the online version of this paper and include the following:

- KEY RESOURCES TABLE
- RESOURCE AVAILABILITY
  - Lead contact
  - Materials availability
  - Data and code availability
- EXPERIMENTAL MODEL AND STUDY PARTICIPANT DETAILS
  - Ethical issues
  - Animals
  - Viral vectors
- METHOD DETAILS
  - Experimental design
  - Stereotaxic AAV injection
  - EEG and EMG surgical procedures
  - Pharmacogenetic manipulation
  - Stress protocols
  - Sleep/wake monitoring
  - Infrared thermography
  - Behavioral tests
  - Anatomical validation of AAV injections
  - *In situ* hybridization (ISH)
  - Immunohistochemistry (IHC)
  - Nomenclature and abbreviations
- QUANTIFICATION AND STATISTICAL ANALYSIS
  - Sleep analysis
  - Image acquisition and processing
  - Quantification of labeling
  - Statistics

SUPPLEMENTAL INFORMATION

Supplemental information can be found online at https://doi.org/10.1016/j.celrep.2024.114411.

ACKNOWLEDGMENTS

We thank the IBPS Behavioral Core Facility for excellent technical assistance and especially Marine Robouam and Jean Vincent; Stéphane Fouquet, David Godefroy, and Marie-Laure Niepon of the Imaging Facility at Institut de la Vision (Sorbonne Université); Susanne Bolte, Jean-François Gilles, and France Lam from the Photon Microscopy Facility of the Institut de Biologie Paris-Seine (Sorbonne Université); Sébastien Parnaudeau for lending us the CD1 aggressors; and undergraduate students Hugo Bonnefou, Eleonore Hardy, Juliette Kallaydjian, Khadija Laurent-Haond, and Kévin Milliet for technical help. We thank Patricia Gaspar and Thierry Gallopin for the stimulating discussions we had throughout this project. We thank BioRender for their assistance in creating the graphical abstract. This research was supported by funds from Institut National de la Santé et de la Recherche Médicale, Centre National de la Recherche Scientifique, Sorbonne Université and Fédération pour la Recherche sur le Cerveau (FRC 2016; Le Sommeil et les Ryhtmes Circadiens). F.H. has benefited from support by the Investissements d'Avenir program managed by the ANR under reference ANR-11-IDEX-0004-02 (Laboratoire d'Excellence de Biologie pour la Psychiatrie, Bio-Psy) and the Société Française de Recherche et Médecine du Sommeil (SFRMS). These funders had no rule in the study design, data collection, and analysis, decision to publish, and preparation of the manuscript.

AUTHOR CONTRIBUTIONS

Conceptualization, F.H., V.F., S.E.M., and S.D.; formal analysis, F.H., V.B., and V.F.; funding acquisition, N.P., S.D., S.E.M., and V.F.; investigation, F.H., S.D., O.P., G.G., V.B., M.P., N.P., S.D., S.E.M., and V.F.; writing – original draft, F.H. and V.F.; writing – review & editing, F.H., S.D., G.G., V.B., N.P., S.D., S.E.M., and V.F.;

DECLARATION OF INTERESTS

The authors declare no competing interests.

DECLARATION OF GENERATIVE AI AND AI-ASSISTED TECHNOLOGIES IN THE WRITING PROCESS

During the preparation of this work, the authors used ChatGPT 3.5 (OpenAI) in order to improve the readability and language of the manuscript. After using this tool, the authors reviewed and edited the content as needed and take full responsibility for the content of the published article.

Received: February 23, 2023
Revised: May 7, 2024
Accepted: June 12, 2024
Published: June 29, 2024

REFERENCES

1. Rachalski, A., Alexandre, C., Bernard, J.-F., Saurini, F., Lesch, K.-P., Hamon, M., Adrien, J., and Fabre, V. (2009). Altered sleep homeostasis after restraint stress in 5-HTT knock-out male mice: a role for hypocretins. J. Neurosci. *29*, 15575–15585. https://doi.org/10.1523/JNEUROSCI.3138-09.2009.
2. Henderson, F., Vialou, V., El Mestikawy, S., and Fabre, V. (2017). Effects of Social Defeat Stress on Sleep in Mice. Front. Behav. Neurosci. *11*, 227. https://doi.org/10.3389/fnbeh.2017.00227.
3. Franklin, T.B., Saab, B.J., and Mansuy, I.M. (2012). Neural mechanisms of stress resilience and vulnerability. Neuron *75*, 747–761. https://doi.org/10.1016/j.neuron.2012.08.016.
4. Paul, E.D., and Lowry, C.A. (2013). Functional topography of serotonergic systems supports the Deakin/Graeff hypothesis of anxiety and affective disorders. J. Psychopharmacol. *27*, 1090–1106. https://doi.org/10.1177/0269881113490328.
5. Houdouin, F., Cespuglio, R., Gharib, A., Sarda, N., and Jouvet, M. (1991). Detection of the release of 5-hydroxyindole compounds in the hypothalamus and the n. raphe dorsalis throughout the sleep-waking cycle and during stressful situations in the rat: a polygraphic and voltammetric approach. Exp. Brain Res. *85*, 153–162.
6. Amat, J., Baratta, M.V., Paul, E., Bland, S.T., Watkins, L.R., and Maier, S.F. (2005). Medial prefrontal cortex determines how stressor controllability affects behavior and dorsal raphe nucleus. Nat. Neurosci. *8*, 365–371. https://doi.org/10.1038/nn1399.
7. Mongeau, R., Martin, C.B.P., Chevarin, C., Maldonado, R., Hamon, M., Robledo, P., and Lanfumey, L. (2010). 5-HT2C receptor activation prevents stress-induced enhancement of brain 5-HT turnover and extracellular levels in the mouse brain: modulation by chronic paroxetine treatment. J. Neurochem. *115*, 438–449. https://doi.org/10.1111/j.1471-4159.2010.06932.x.
8. Ahnaou, A., and Drinkenburg, W.H.I.M. (2016). Simultaneous Changes in Sleep, qEEG, Physiology, Behaviour and Neurochemistry in Rats Exposed to Repeated Social Defeat Stress. Neuropsychobiology *73*, 209–223. https://doi.org/10.1159/000446284.
9. Cespuglio, R., Marinesco, S., Baubet, V., Bonnet, C., and el Kafi, B. (1995). Evidence for a sleep-promoting influence of stress. Adv. Neuroimmunol. *5*, 145–154. https://doi.org/10.1016/0960-5428(95)00005-m.
10. Boutrel, B., Monaca, C., Hen, R., Hamon, M., and Adrien, J. (2002). Involvement of 5-HT1A receptors in homeostatic and stress-induced adaptive regulations of paradoxical sleep: studies in 5-HT1A knock-out mice. J. Neurosci. *22*, 4686–4692. https://doi.org/10.1523/JNEUROSCI.22-11-04686.2002.
11. Gaspar, P., and Lillesaar, C. (2012). Probing the diversity of serotonin neurons. Philos. Trans. R. Soc. Lond. B Biol. Sci. *367*, 2382–2394. https://doi.org/10.1098/rstb.2011.0378.
12. Okaty, B.W., Commons, K.G., and Dymecki, S.M. (2019). Embracing diversity in the 5-HT neuronal system. Nat. Rev. Neurosci. *20*, 397–424. https://doi.org/10.1038/s41583-019-0151-3.
13. Huang, K.W., Ochandarena, N.E., Philson, A.C., Hyun, M., Birnbaum, J.E., Cicconet, M., and Sabatini, B.L. (2019). Molecular and anatomical organization of the dorsal raphe nucleus. Elife *8*, e46464. https://doi.org/10.7554/eLife.46464.
14. Ren, J., Isakova, A., Friedmann, D., Zeng, J., Grutzner, S.M., Pun, A., Zhao, G.Q., Kolluru, S.S., Wang, R., Lin, R., et al. (2019). Single-cell transcriptomes and whole-brain projections of serotonin neurons in the mouse dorsal and median raphe nuclei. Elife *8*, e49424. https://doi.org/10.7554/eLife.49424.
15. Okaty, B.W., Sturrock, N., Escobedo Lozoya, Y., Chang, Y., Senft, R.A., Lyon, K.A., Alekseyenko, O.V., and Dymecki, S.M. (2020). A single-cell transcriptomic and anatomic atlas of mouse dorsal raphe Pet1 neurons. Elife *9*, e55523. https://doi.org/10.7554/eLife.55523.
16. Muzerelle, A., Scotto-Lomassese, S., Bernard, J.F., Soiza-Reilly, M., and Gaspar, P. (2016). Conditional anterograde tracing reveals distinct targeting of individual serotonin cell groups (B5-B9) to the forebrain and brainstem. Brain Struct. Funct. *221*, 535–561. https://doi.org/10.1007/s00429-014-0924-4.
17. Ren, J., Friedmann, D., Xiong, J., Liu, C.D., Ferguson, B.R., Weerakkody, T., DeLoach, K.E., Ran, C., Pun, A., Sun, Y., et al. (2018). Anatomically Defined and Functionally Distinct Dorsal Raphe Serotonin Sub-systems. Cell *175*, 472–487.e20. https://doi.org/10.1016/j.cell.2018.07.043.
18. Allers, K.A., and Sharp, T. (2003). Neurochemical and anatomical identification of fast- and slow-firing neurones in the rat dorsal raphe nucleus using juxtacellular labelling methods in vivo. Neuroscience *122*, 193–204. https://doi.org/10.1016/s0306-4522(03)00518-9.
19. Kocsis, B., Varga, V., Dahan, L., and Sik, A. (2006). Serotonergic neuron diversity: identification of raphe neurons with discharges time-locked to the hippocampal theta rhythm. Proc. Natl. Acad. Sci. USA *103*, 1059–1064. https://doi.org/10.1073/pnas.0508360103.
20. Fernandez, S.P., Cauli, B., Cabezas, C., Muzerelle, A., Poncer, J.-C., and Gaspar, P. (2016). Multiscale single-cell analysis reveals unique

phenotypes of raphe 5-HT neurons projecting to the forebrain. Brain Struct. Funct. *221*, 4007–4025. https://doi.org/10.1007/s00429-015-1142-4.

21. Fu, W., Le Maître, E., Fabre, V., Bernard, J.-F., David Xu, Z.-Q., and Hökfelt, T. (2010). Chemical neuroanatomy of the dorsal raphe nucleus and adjacent structures of the mouse brain. J. Comp. Neurol. *518*, 3464–3494. https://doi.org/10.1002/cne.22407.
22. Yu, X.-D., Zhu, Y., Sun, Q.-X., Deng, F., Wan, J., Zheng, D., Gong, W., Xie, S.-Z., Shen, C.-J., Fu, J.-Y., et al. (2022). Distinct serotonergic pathways to the amygdala underlie separate behavioral features of anxiety. Nat. Neurosci. *25*, 1651–1663. https://doi.org/10.1038/s41593-022-01200-8.
23. Zou, W.-J., Song, Y.-L., Wu, M.-Y., Chen, X.-T., You, Q.-L., Yang, Q., Luo, Z.-Y., Huang, L., Kong, Y., Feng, J., et al. (2020). A discrete serotonergic circuit regulates vulnerability to social stress. Nat. Commun. *11*, 4218. https://doi.org/10.1038/s41467-020-18010-w.
24. Challis, C., Boulden, J., Veerakumar, A., Espallergues, J., Vassoler, F.M., Pierce, R.C., Beck, S.G., and Berton, O. (2013). Raphe GABAergic neurons mediate the acquisition of avoidance after social defeat. J. Neurosci. *33*, 13978–13988. https://doi.org/10.1523/JNEUROSCI.2383-13.2013.
25. Cho, J.R., Treweek, J.B., Robinson, J.E., Xiao, C., Bremner, L.R., Greenbaum, A., and Gradinaru, V. (2017). Dorsal Raphe Dopamine Neurons Modulate Arousal and Promote Wakefulness by Salient Stimuli. Neuron *94*, 1205–1219.e8. https://doi.org/10.1016/j.neuron.2017.05.020.
26. Gazea, M., Furdan, S., Sere, P., Oesch, L., Molnár, B., Di Giovanni, G., Fenno, L.E., Ramakrishnan, C., Mattis, J., Deisseroth, K., et al. (2021). Reciprocal Lateral Hypothalamic and Raphe GABAergic Projections Promote Wakefulness. J. Neurosci. *41*, 4840–4849. https://doi.org/10.1523/JNEUROSCI.2850-20.2021.
27. Varga, V., Losonczy, A., Zemelman, B.V., Borhegyi, Z., Nyiri, G., Domonkos, A., Hangya, B., Holderith, N., Magee, J.C., and Freund, T.F. (2009). Fast synaptic subcortical control of hippocampal circuits. Science *326*, 449–453. https://doi.org/10.1126/science.1178307.
28. Kapoor, V., Provost, A.C., Agarwal, P., and Murthy, V.N. (2016). Activation of raphe nuclei triggers rapid and distinct effects on parallel olfactory bulb output channels. Nat. Neurosci. *19*, 271–282. https://doi.org/10.1038/nn.4219.
29. Sengupta, A., Bocchio, M., Bannerman, D.M., Sharp, T., and Capogna, M. (2017). Control of Amygdala Circuits by 5-HT Neurons via 5-HT and Glutamate Cotransmission. J. Neurosci. *37*, 1785–1796. https://doi.org/10.1523/JNEUROSCI.2238-16.2016.
30. Wang, H.-L., Zhang, S., Qi, J., Wang, H., Cachope, R., Mejias-Aponte, C.A., Gomez, J.A., Mateo-Semidey, G.E., Beaudoin, G.M.J., Paladini, C.A., et al. (2019). Dorsal Raphe Dual Serotonin-Glutamate Neurons Drive Reward by Establishing Excitatory Synapses on VTA Mesoaccumbens Dopamine Neurons. Cell Rep. *26*, 1128–1142.e7. https://doi.org/10.1016/j.celrep.2019.01.014.
31. Gras, C., Amilhon, B., Lepicard, E.M., Poirel, O., Vinatier, J., Herbin, M., Dumas, S., Tzavara, E.T., Wade, M.R., Nomikos, G.G., et al. (2008). The vesicular glutamate transporter VGLUT3 synergizes striatal acetylcholine tone. Nat. Neurosci. *11*, 292–300. https://doi.org/10.1038/nn2052.
32. Amilhon, B., Lepicard, E., Renoir, T., Mongeau, R., Popa, D., Poirel, O., Miot, S., Gras, C., Gardier, A.M., Gallego, J., et al. (2010). VGLUT3 (vesicular glutamate transporter type 3) contribution to the regulation of serotonergic transmission and anxiety. J. Neurosci. *30*, 2198–2210. https://doi.org/10.1523/JNEUROSCI.5196-09.2010.
33. Favier, M., Pietrancosta, N., El Mestikawy, S., and Gangarossa, G. (2021). Leveraging VGLUT3 Functions to Untangle Brain Dysfunctions. Trends Pharmacol. Sci. *42*, 475–490. https://doi.org/10.1016/j.tips.2021.03.003.
34. McDevitt, R.A., Tiran-Cappello, A., Shen, H., Balderas, I., Britt, J.P., Marino, R.A.M., Chung, S.L., Richie, C.T., Harvey, B.K., and Bonci, A. (2014). Serotonergic versus nonserotonergic dorsal raphe projection neurons: differential participation in reward circuitry. Cell Rep. *8*, 1857–1869. https://doi.org/10.1016/j.celrep.2014.08.037.
35. Qi, J., Zhang, S., Wang, H.-L., Wang, H., de Jesus Aceves Buendia, J., Hoffman, A.F., Lupica, C.R., Seal, R.P., and Morales, M. (2014). A glutamatergic reward input from the dorsal raphe to ventral tegmental area dopamine neurons. Nat. Commun. *5*, 5390. https://doi.org/10.1038/ncomms6390.
36. Liu, Z., Zhou, J., Li, Y., Hu, F., Lu, Y., Ma, M., Feng, Q., Zhang, J.-E., Wang, D., Zeng, J., et al. (2014). Dorsal raphe neurons signal reward through 5-HT and glutamate. Neuron *81*, 1360–1374. https://doi.org/10.1016/j.neuron.2014.02.010.
37. Fontaine, H.M., Silva, P.R., Neiswanger, C., Tran, R., Abraham, A.D., Land, B.B., Neumaier, J.F., and Chavkin, C. (2022). Stress decreases serotonin tone in the nucleus accumbens in male mice to promote aversion and potentiate cocaine preference via decreased stimulation of 5-HT1B receptors. Neuropsychopharmacology *47*, 891–901. https://doi.org/10.1038/s41386-021-01178-0.
38. Nectow, A.R., Schneeberger, M., Zhang, H., Field, B.C., Renier, N., Azevedo, E., Patel, B., Liang, Y., Mitra, S., Tessier-Lavigne, M., et al. (2017). Identification of a Brainstem Circuit Controlling Feeding. Cell *170*, 429–442.e11. https://doi.org/10.1016/j.cell.2017.06.045.
39. Schneeberger, M., Brice, N.L., Pellegrino, K., Parolari, L., Shaked, J.T., Page, K.J., Marchildon, F., Barrows, D.W., Carroll, T.S., Topilko, T., et al. (2022). Pharmacological targeting of glutamatergic neurons within the brainstem for weight reduction. Nat. Metab. *4*, 1495–1513. https://doi.org/10.1038/s42255-022-00677-8.
40. Wang, X.-Y., Jia, W.-B., Xu, X., Chen, R., Wang, L.-B., Su, X.-J., Xu, P.-F., Liu, X.-Q., Wen, J., Song, X.-Y., et al. (2023). A glutamatergic DRN-VTA pathway modulates neuropathic pain and comorbid anhedonia-like behavior in mice. Nat. Commun. *14*, 5124. https://doi.org/10.1038/s41467-023-40860-3.
41. Hioki, H., Nakamura, H., Ma, Y.-F., Konno, M., Hayakawa, T., Nakamura, K.C., Fujiyama, F., and Kaneko, T. (2010). Vesicular glutamate transporter 3-expressing nonserotonergic projection neurons constitute a subregion in the rat midbrain raphe nuclei. J. Comp. Neurol. *518*, 668–686. https://doi.org/10.1002/cne.22237.
42. Senft, R.A., Freret, M.E., Sturrock, N., and Dymecki, S.M. (2021). Neurochemically and Hodologically Distinct Ascending VGLUT3 versus Serotonin Subsystems Comprise the r2-Pet1 Median Raphe. J. Neurosci. *41*, 2581–2600. https://doi.org/10.1523/JNEUROSCI.1667-20.2021.
43. Franklin, K.B.J., and Paxinos, G. (2008). The Mouse Brain in Stereotaxic Coordinates Third Edition 2008 (Elsevier).
44. Ulrich-Lai, Y.M., and Herman, J.P. (2009). Neural regulation of endocrine and autonomic stress responses. Nat. Rev. Neurosci. *10*, 397–409. https://doi.org/10.1038/nrn2647.
45. Sulaman, B.A., Wang, S., Tyan, J., and Eban-Rothschild, A. (2023). Neuro-orchestration of sleep and wakefulness. Nat. Neurosci. *26*, 196–212. https://doi.org/10.1038/s41593-022-01236-w.
46. Kaur, S., Pedersen, N.P., Yokota, S., Hur, E.E., Fuller, P.M., Lazarus, M., Chamberlin, N.L., and Saper, C.B. (2013). Glutamatergic signaling from the parabrachial nucleus plays a critical role in hypercapnic arousal. J. Neurosci. *33*, 7627–7640. https://doi.org/10.1523/JNEUROSCI.0173-13.2013.
47. Eban-Rothschild, A., Rothschild, G., Giardino, W.J., Jones, J.R., and de Lecea, L. (2016). VTA dopaminergic neurons regulate ethologically relevant sleep-wake behaviors. Nat. Neurosci. *19*, 1356–1366. https://doi.org/10.1038/nn.4377.
48. Luo, Y.-J., Li, Y.-D., Wang, L., Yang, S.-R., Yuan, X.-S., Wang, J., Cherasse, Y., Lazarus, M., Chen, J.-F., Qu, W.-M., and Huang, Z.L. (2018). Nucleus accumbens controls wakefulness by a subpopulation of neurons expressing dopamine D1 receptors. Nat. Commun. *9*, 1576. https://doi.org/10.1038/s41467-018-03889-3.
49. Fasano, C., Rocchetti, J., Pietrajtis, K., Zander, J.-F., Manseau, F., Sakae, D.Y., Marcus-Sells, M., Ramet, L., Morel, L.J., Carrel, D., et al. (2017). Regulation of the Hippocampal Network by VGLUT3-Positive

CCK- GABAergic Basket Cells. Front. Cell. Neurosci. *11*, 140. https://doi.org/10.3389/fncel.2017.00140.

50. Murray, N.M., Buchanan, G.F., and Richerson, G.B. (2015). Insomnia Caused by Serotonin Depletion is Due to Hypothermia. Sleep *38*, 1985–1993. https://doi.org/10.5665/sleep.5256.

51. Meerlo, P., and Turek, F.W. (2001). Effects of social stimuli on sleep in mice: non-rapid-eye-movement (NREM) sleep is promoted by aggressive interaction but not by sexual interaction. Brain Res. *907*, 84–92. https://doi.org/10.1016/s0006-8993(01)02603-8.

52. Yu, X., Zhao, G., Wang, D., Wang, S., Li, R., Li, A., Wang, H., Nollet, M., Chun, Y.Y., Zhao, T., et al. (2022). A specific circuit in the midbrain detects stress and induces restorative sleep. Science *377*, 63–72. https://doi.org/10.1126/science.abn0853.

53. Geisler, S., Derst, C., Veh, R.W., and Zahm, D.S. (2007). Glutamatergic afferents of the ventral tegmental area in the rat. J. Neurosci. *27*, 5730–5743. https://doi.org/10.1523/JNEUROSCI.0012-07.2007.

54. Niu, M., Kasai, A., Tanuma, M., Seiriki, K., Igarashi, H., Kuwaki, T., Nagayasu, K., Miyaji, K., Ueno, H., Tanabe, W., et al. (2022). Claustrum mediates bidirectional and reversible control of stress-induced anxiety responses. Sci. Adv. *8*, eabi6375. https://doi.org/10.1126/sciadv.abi6375.

55. Houdouin, F., Cespuglio, R., and Jouvet, M. (1991). Effects induced by the electrical stimulation of the nucleus raphe dorsalis upon hypothalamic release of 5-hydroxyindole compounds and sleep parameters in the rat. Brain Res. *565*, 48–56. https://doi.org/10.1016/0006-8993(91)91735-j.

56. Lkhagvasuren, B., Nakamura, Y., Oka, T., Sudo, N., and Nakamura, K. (2011). Social defeat stress induces hyperthermia through activation of thermoregulatory sympathetic premotor neurons in the medullary raphe region. Eur. J. Neurosci. *34*, 1442–1452. https://doi.org/10.1111/j.1460-9568.2011.07863.x.

57. Machado, N.L.S., Abbott, S.B.G., Resch, J.M., Zhu, L., Arrigoni, E., Lowell, B.B., Fuller, P.M., Fontes, M.A.P., and Saper, C.B. (2018). A Glutamatergic Hypothalamomedullary Circuit Mediates Thermogenesis, but Not Heat Conservation, during Stress-Induced Hyperthermia. Curr. Biol. *28*, 2291–2301.e5. https://doi.org/10.1016/j.cub.2018.05.064.

58. Fabre, V., Krystal, A., and Bonnavion, P. (2021). Serotonin and sleep. In Principles and Practice of Sleep Medicine, 7th edition., M.H. Kryger, T. Roth, C.A. Goldstein, and W.C. Dement, eds. (Elsevier), pp. 497–505.

59. Varin, C., Luppi, P.-H., and Fort, P. (2018). Melanin-concentrating hormone-expressing neurons adjust slow-wave sleep dynamics to catalyze paradoxical (REM) sleep. Sleep *41*, zsy068. https://doi.org/10.1093/sleep/zsy068.

60. Traut, J., Mengual, J.P., Meijer, E.J., McKillop, L.E., Alfonsa, H., Hoerder-Suabedissen, A., Song, S.M., Molnár, Z., Akerman, C.J., Vyazovskiy, V.V., et al. (2022). Effects of clozapine-N-oxide and compound 21 on sleep in laboratory mice. Preprint at bioRxiv. https://doi.org/10.1101/2022.02.01.478652.

61. Fazekas, C.L., Szabó, A., Török, B., Bánrévi, K., Correia, P., Chaves, T., Daumas, S., and Zelena, D. (2022). A New Player in the Hippocampus: A Review on VGLUT3+ Neurons and Their Role in the Regulation of Hippocampal Activity and Behaviour. Int. J. Mol. Sci. *23*, 790. https://doi.org/10.3390/ijms23020790.

62. Domonkos, A., Nikitidou Ledri, L., Laszlovszky, T., Cserép, C., Borhegyi, Z., Papp, E., Nyiri, G., Freund, T.F., and Varga, V. (2016). Divergent in vivo activity of non-serotonergic and serotonergic VGluT3-neurones in the median raphe region. J. Physiol. *594*, 3775–3790. https://doi.org/10.1113/JP272036.

63. Marinesco, S., Bonnet, C., and Cespuglio, R. (1999). Influence of stress duration on the sleep rebound induced by immobilization in the rat: a possible role for corticosterone. Neuroscience *92*, 921–933. https://doi.org/10.1016/s0306-4522(99)00045-7.

64. Fujii, S., Kaushik, M.K., Zhou, X., Korkutata, M., and Lazarus, M. (2019). Acute Social Defeat Stress Increases Sleep in Mice. Front. Neurosci. *13*, 322. https://doi.org/10.3389/fnins.2019.00322.

65. Cohen, J.Y., Amoroso, M.W., and Uchida, N. (2015). Serotonergic neurons signal reward and punishment on multiple timescales. Elife *4*, e06346. https://doi.org/10.7554/eLife.06346.

66. Matthews, G.A., Nieh, E.H., Vander Weele, C.M., Halbert, S.A., Pradhan, R.V., Yosafat, A.S., Glober, G.F., Izadmehr, E.M., Thomas, R.E., Lacy, G.D., et al. (2016). Dorsal Raphe Dopamine Neurons Represent the Experience of Social Isolation. Cell *164*, 617–631. https://doi.org/10.1016/j.cell.2015.12.040.

67. Groessl, F., Munsch, T., Meis, S., Griessner, J., Kaczanowska, J., Pliota, P., Kargl, D., Badurek, S., Kraitsy, K., Rassoulpour, A., et al. (2018). Dorsal tegmental dopamine neurons gate associative learning of fear. Nat. Neurosci. *21*, 952–962. https://doi.org/10.1038/s41593-018-0174-5.

68. Paquelet, G.E., Carrion, K., Lacefield, C.O., Zhou, P., Hen, R., and Miller, B.R. (2022). Single-cell activity and network properties of dorsal raphe nucleus serotonin neurons during emotionally salient behaviors. Neuron *110*, 2664–2679.e8. https://doi.org/10.1016/j.neuron.2022.05.015.

69. Lin, R., Liang, J., Wang, R., Yan, T., Zhou, Y., Liu, Y., Feng, Q., Sun, F., Li, Y., Li, A., et al. (2020). The Raphe Dopamine System Controls the Expression of Incentive Memory. Neuron *106*, 498–514.e8. https://doi.org/10.1016/j.neuron.2020.02.009.

70. Hokari, S., Chikahisa, S., Shiuchi, T., Nakayama, Y., Konishi, M., Nishino, S., Itoh, N., and Séi, H. (2022). Social stress alters sleep in FGF21-deficient mice. Brain Res. Bull. *191*, 40–47. https://doi.org/10.1016/j.brainresbull.2022.10.005.

71. Koehl, M., Bouyer, J.J., Darnaudéry, M., Le Moal, M., and Mayo, W. (2002). The effect of restraint stress on paradoxical sleep is influenced by the circadian cycle. Brain Res. *937*, 45–50. https://doi.org/10.1016/s0006-8993(02)02463-0.

72. Meerlo, P., Easton, A., Bergmann, B.M., and Turek, F.W. (2001). Restraint increases prolactin and REM sleep in C57BL/6J mice but not in BALB/cJ mice. Am. J. Physiol. Regul. Integr. Comp. Physiol. *281*, R846–R854. https://doi.org/10.1152/ajpregu.2001.281.3.R846.

73. Vazquez-Palacios, G., and Velazquez-Moctezuma, J. (2000). Effect of electric foot shocks, immobilization, and corticosterone administration on the sleep-wake pattern in the rat. Physiol. Behav. *71*, 23–28. https://doi.org/10.1016/s0031-9384(00)00285-7.

74. Bush, B.J., Donnay, C., Andrews, E.-J.A., Lewis-Sanders, D., Gray, C.L., Qiao, Z., Brager, A.J., Johnson, H., Brewer, H.C.S., Sood, S., et al. (2022). Non-rapid eye movement sleep determines resilience to social stress. Elife *11*, e80206. https://doi.org/10.7554/eLife.80206.

75. Feng, X., Zhao, H.-Y., Shao, Y.-J., Lou, H.-F., Zhu, L.-Y., Duan, S., and Yu, Y.-Q. (2020). Anxiolytic Effect of Increased NREM Sleep after Acute Social Defeat Stress in Mice. Neurosci. Bull. *36*, 1137–1146. https://doi.org/10.1007/s12264-020-00473-y.

76. Nagai, M., Nagai, H., Numa, C., and Furuyashiki, T. (2020). Stress-induced sleep-like inactivity modulates stress susceptibility in mice. Sci. Rep. *10*, 19800. https://doi.org/10.1038/s41598-020-76717-8.

77. Goldstein, A.N., and Walker, M.P. (2014). The role of sleep in emotional brain function. Annu. Rev. Clin. Psychol. *10*, 679–708. https://doi.org/10.1146/annurev-clinpsy-032813-153716.

78. Wassing, R., Lakbila-Kamal, O., Ramautar, J.R., Stoffers, D., Schalkwijk, F., and Van Someren, E.J.W. (2019). Restless REM Sleep Impedes Overnight Amygdala Adaptation. Curr. Biol. *29*, 2351–2358.e4. https://doi.org/10.1016/j.cub.2019.06.034.

79. Aime, M., Calcini, N., Borsa, M., Campelo, T., Rusterholz, T., Sattin, A., Fellin, T., and Adamantidis, A. (2022). Paradoxical somatodendritic decoupling supports cortical plasticity during REM sleep. Science *376*, 724–730. https://doi.org/10.1126/science.abk2734.

80. Popa, D., Duvarci, S., Popescu, A.T., Léna, C., and Paré, D. (2010). Coherent amygdalocortical theta promotes fear memory consolidation

during paradoxical sleep. Proc. Natl. Acad. Sci. USA *107*, 6516–6519. https://doi.org/10.1073/pnas.0913016107.

81. Boyce, R., Glasgow, S.D., Williams, S., and Adamantidis, A. (2016). Causal evidence for the role of REM sleep theta rhythm in contextual memory consolidation. Science *352*, 812–816. https://doi.org/10.1126/science.aad5252.
82. Balázsfi, D., Fodor, A., Török, B., Ferenczi, S., Kovács, K.J., Haller, J., and Zelena, D. (2018). Enhanced innate fear and altered stress axis regulation in VGluT3 knockout mice. Stress Amst. Neth. *21*, 151–161. https://doi.org/10.1080/10253890.2017.1423053.
83. de Almeida, C., Chabbah, N., Eyraud, C., Fasano, C., Bernard, V., Pietrancosta, N., Fabre, V., El Mestikawy, S., and Daumas, S. (2023). Absence of VGLUT3 expression leads to impaired fear memory in mice. eNeuro *10*. https://doi.org/10.1523/ENEURO.0304-22.2023.
84. Cardozo Pinto, D.F., Yang, H., Pollak Dorocic, I., de Jong, J.W., Han, V.J., Peck, J.R., Zhu, Y., Liu, C., Beier, K.T., Smidt, M.P., and Lammel, S. (2019). Characterization of transgenic mouse models targeting neuromodulatory systems reveals organizational principles of the dorsal raphe. Nat. Commun. *10*, 4633. https://doi.org/10.1038/s41467-019-12392-2.
85. Sengupta, A., and Holmes, A. (2019). A Discrete Dorsal Raphe to Basal Amygdala 5-HT Circuit Calibrates Aversive Memory. Neuron *103*, 489–505.e7. https://doi.org/10.1016/j.neuron.2019.05.029.
86. Gullino, L.S., Fuller, C., Dunn, P., Collins, H.M., El Mestikawy, S., and Sharp, T. (2024). Evidence for a Role of 5-HT-glutamate Co-releasing Neurons in Acute Stress Mechanisms. ACS Chem. Neurosci. *15*, 1185–1196. https://doi.org/10.1021/acschemneuro.3c00758.
87. Sakai, K. (2011). Sleep-waking discharge profiles of dorsal raphe nucleus neurons in mice. Neuroscience *197*, 200–224. https://doi.org/10.1016/j.neuroscience.2011.09.024.
88. Andrade, T.G., Zangrossi, H., and Graeff, F.G. (2013). The median raphe nucleus in anxiety revisited. J. Psychopharmacol. *27*, 1107–1115. https://doi.org/10.1177/0269881113499208.
89. Bernabe, C.S., Caliman, I.F., de Abreu, A.R.R., Molosh, A.I., Truitt, W.A., Shekhar, A., and Johnson, P.L. (2024). Identification of a novel perifornical-hypothalamic-area-projecting serotonergic system that inhibits innate panic and conditioned fear responses. Transl. Psychiatry *14*, 60. https://doi.org/10.1038/s41398-024-02769-3.
90. Urbain, N., Creamer, K., and Debonnel, G. (2006). Electrophysiological diversity of the dorsal raphe cells across the sleep-wake cycle of the rat. J. Physiol. *573*, 679–695. https://doi.org/10.1113/jphysiol.2006.108514.
91. Oishi, Y., Xu, Q., Wang, L., Zhang, B.-J., Takahashi, K., Takata, Y., Luo, Y.-J., Cherasse, Y., Schiffmann, S.N., de Kerchove d'Exaerde, A., et al. (2017). Slow-wave sleep is controlled by a subset of nucleus accumbens core neurons in mice. Nat. Commun. *8*, 734. https://doi.org/10.1038/s41467-017-00781-4.
92. Carter, M.E., Brill, J., Bonnavion, P., Huguenard, J.R., Huerta, R., and de Lecea, L. (2012). Mechanism for Hypocretin-mediated sleep-to-wake transitions. Proc. Natl. Acad. Sci. USA *109*, E2635–E2644. https://doi.org/10.1073/pnas.1202526109.
93. Anaclet, C., Pedersen, N.P., Ferrari, L.L., Venner, A., Bass, C.E., Arrigoni, E., and Fuller, P.M. (2015). Basal forebrain control of wakefulness and cortical rhythms. Nat. Commun. *6*, 8744. https://doi.org/10.1038/ncomms9744.
94. Krone, L.B., Yamagata, T., Blanco-Duque, C., Guillaumin, M.C.C., Kahn, M.C., van der Vinne, V., McKillop, L.E., Tam, S.K.E., Peirson, S.N., Akerman, C.J., et al. (2021). A role for the cortex in sleep-wake regulation. Nat. Neurosci. *24*, 1210–1215. https://doi.org/10.1038/s41593-021-00894-6.
95. Hasegawa, E., Miyasaka, A., Sakurai, K., Cherasse, Y., Li, Y., and Sakurai, T. (2022). Rapid eye movement sleep is initiated by basolateral amygdala dopamine signaling in mice. Science *375*, 994–1000. https://doi.org/10.1126/science.abl6618.
96. Fuller, P.M., Sherman, D., Pedersen, N.P., Saper, C.B., and Lu, J. (2011). Reassessment of the structural basis of the ascending arousal system. J. Comp. Neurol. *519*, 933–956. https://doi.org/10.1002/cne.22559.
97. Yu, X., Li, W., Ma, Y., Tossell, K., Harris, J.J., Harding, E.C., Ba, W., Miracca, G., Wang, D., Li, L., et al. (2019). GABA and glutamate neurons in the VTA regulate sleep and wakefulness. Nat. Neurosci. *22*, 106–119. https://doi.org/10.1038/s41593-018-0288-9.
98. Berton, O., McClung, C.A., Dileone, R.J., Krishnan, V., Renthal, W., Russo, S.J., Graham, D., Tsankova, N.M., Bolanos, C.A., Rios, M., et al. (2006). Essential role of BDNF in the mesolimbic dopamine pathway in social defeat stress. Science *311*, 864–868. https://doi.org/10.1126/science.1120972.
99. Mang, G.M., and Franken, P. (2012). Sleep and EEG Phenotyping in Mice. Curr Protoc Mouse Biol. *2*, 55–74. https://doi.org/10.1002/9780470942390.mo110126.
100. Zhuang, X., Masson, J., Gingrich, J.A., Rayport, S., and Hen, R. (2005). Targeted gene expression in dopamine and serotonin neurons of the mouse brain. J. Neurosci. Methods *143*, 27–32. https://doi.org/10.1016/j.jneumeth.2004.09.020.
101. Roth, B.L. (2016). DREADDs for Neuroscientists. Neuron *89*, 683–694. https://doi.org/10.1016/j.neuron.2016.01.040.
102. Srinivas, S., Watanabe, T., Lin, C.S., William, C.M., Tanabe, Y., Jessell, T.M., and Costantini, F. (2001). Cre reporter strains produced by targeted insertion of EYFP and ECFP into the ROSA26 locus. BMC Dev. Biol. *1*, 4.
103. Bimpisidis, Z., König, N., Stagkourakis, S., Zell, V., Vlcek, B., Dumas, S., Giros, B., Broberger, C., Hnasko, T.S., and Mackenzie, Å. (2019). The NeuroD6 Subtype of VTA Neurons Contributes to Psychostimulant Sensitization and Behavioral Reinforcement. eNeuro *6*. https://doi.org/10.1523/ENEURO.0066-19.2019.
104. Dumas, S., and Wallén-Mackenzie, Å. (2019). Developmental Co-expression of Vglut2 and Nurr1 in a Mes-Di-Encephalic Continuum Preceeds Dopamine and Glutamate Neuron Specification. Front. Cell Dev. Biol. *7*, 307. https://doi.org/10.3389/fcell.2019.00307.
105. Serra, G.P., Guillaumin, A., Dumas, S., Vlcek, B., and Wallén-Mackenzie, Å. (2021). Midbrain Dopamine Neurons Defined by TrpV1 Modulate Psychomotor Behavior. Front. Neural Circ. *15*, 726893. https://doi.org/10.3389/fncir.2021.726893.
106. Bonnavion, P., Bernard, J.-F., Hamon, M., Adrien, J., and Fabre, V. (2010). Heterogeneous distribution of the serotonin 5-HT(1A) receptor mRNA in chemically identified neurons of the mouse rostral brainstem: Implications for the role of serotonin in the regulation of wakefulness and REM sleep. J. Comp. Neurol. *518*, 2744–2770. https://doi.org/10.1002/cne.22331.

STAR★METHODS

KEY RESOURCES TABLE

REAGENT or RESOURCE	SOURCE	IDENTIFIER
Antibodies		
Rabbit polyclonal anti-*c*-Fos	Abcam	Cat# 190289; RRID: AB_2737414
Chicken polyclonal anti-GFP	Aves Labs	Cat# 1020; RRID: AB_10000240
Mouse monoclonal (WH-3) anti-TPH2	Sigma-Aldrich	Cat# T0678; RRID:AB_261587
Mouse monoclonal (CL2990) anti-TPH2	Abcam	Cat# 211528-1001; RRID: AB_2313773
Biotinylated anti-rabbit IgG	Vector Laboratories	Cat#PI-1000; RRID: AB_2313606
Alexa Fluor 594 anti-rabbit IgG	Thermo Fisher Scientific	Cat# A-21207; RRID: AB_141637
Alexa Fluor 488 anti-chicken IgY	Thermo Fisher Scientific	Cat# A32931; RRID: AB_2762843
Abberior-Star 635P anti-mouse IgG	Abberior	Cat# ST635-1001; RRID: AB_2893232
HRP conjugated anti-fluorescein antibody	Roche, Mannheim	Cat# 11426346910; RRID: AB_840257
HRP anti-DIG Fab fragments	Roche, Mannheim	Cat# 11207733910; RRID: AB_514500
Alkaline phosphatase anti-Dig antibody	Roche, Mannheim	Cat# 11093274910; RRID: AB_514497
Bacterial and virus strains		
AAV-DIO-hM3D(Gq)-mCh	UZH Vector Facility	Cat# V89
AAV-DIO-mCh	UZH Vector Facility	Cat# V84
ssAAV-retro/2-hSyn1-dlox-EGFP(rev)-dlox-WPRE-hGHp(A)	UZH Vector Facility	Cat# V115-Retro
AAV-Cre-eGFP	Penn Vector Core	Cat# AV-1-PV2004
AAV-eGFP	Penn Vector Core	Cat# AV-1-PV0101
AAV-Flex-tdTomato	Penn Vector Core	Cat# AV-1-ALL864
Chemicals, peptides, and recombinant proteins		
Clozapine-N-oxide (CNO)	Tocris	Cat# 4936
Experimental models: Organisms/strains		
Mouse: VGLUT3$^{lox/lox}$: C57BL/6N-Slc17a8tm2Selm	Generated by lab of El Mestikawy[98]	RRID: IMSR_EM:05733
Mouse: VGLUT3^{Cre}	This paper	
Mouse: SERT^{Cre}: B6.129(Cg)-Slc6a4tm1(cre)Xz/J	The Jackson Laboratory	JAX #01455
Mouse: VIAAT^{Cre}: Slc32a1tm2(cre)Lowl/J	The Jackson Laboratory	JAX #016962
Mouse: ChAT^{Cre}: B6.129S6-Chattm2(cre)Lowl/J	The Jackson Laboratory	JAX #006410
Mouse: R26-stop-EYFP: B6.129X1-Gt(ROSA)26Sortm1(EYFP)Cos/J	The Jackson Laboratory	JAX #006148
Oligonucleotides		
HIS probe 1 VGLUT3 forward AATTAACCCTCACTAAAGGG AGAAAAACAGGACTGGGCTGACCC	eurogentech	N/A
HIS probe 1 VGLUT3 reverse TAATACGACTCACTATAGGGA GAGAGACCAAGGTCCATATTCCC	eurogentech	N/A
HIS probe 2 VGLUT3 forward AATTAACCCTCACTAAAGGG AGGAGACTCGCTGGGCATC T	eurogentech	N/A
HIS probe 2 VGLUT3 reverse TAATACGACTCACTATAGGGC AGCTGCAGTCACAGATGTACCG	eurogentech	N/A
HIS probe TPH2 forward AATTAACCCTCACTAAAG GGACAAAGAGCCCGGCAAAGGCG	eurogentech	N/A

(*Continued on next page*)

Continued		
REAGENT or RESOURCE	SOURCE	IDENTIFIER
HIS probe TPH2 reverse TAATACGACTCACTATAGGGC TGCTCCATACGCCCGCAGT	eurogentech	N/A
HIS probe Cre forward AATTAACCCTCAC TAAAGGGATCTGTCCGTTTGCCGGTCGTG	eurogentech	N/A
HIS probe Cre reverse TAATACGACTCACT ATAGGGTTGGTCCAGCCACCAGCTTGC	eurogentech	N/A
Software and algorithms		
Somnologica-3	EMBLA, Medcare Flaga	Mang et al.[99]
NDP.view2 Image viewing software	Hamamatsu Photonics	https://nanozoomer.hamamatsu.com/
FLIR-Tools Software	West Malling	RRID:SCR_016330; https://www.flir.fr/
Fiji	ImageJ2	RRID:SCR_002285; https://imagej.net/software/fiji/
GraphPad Prism 7.0	GraphPad Software	RRID:SCR_002798; https://www.graphpad.com/
QuPath v0.5		RRID:SCR_018257; https://qupath.github.io/
EthoVision XT	Noldus	RRID:SCR_000441; https://www.noldus.com/ethovision
Photoshop	Adobe Systems	RRID:SCR_014199; https://www.adobe.com/
Adobe Illustrator	Adobe Systems	RRID: SCR_010279; https://www.adobe.com/

RESOURCE AVAILABILITY

Lead contact

Further information and requests for resources and reagents should be directed to and will be fulfilled by the lead contact, Véronique Fabre (veronique.fabre@inserm.fr).

Materials availability

Unique resources and reagents generated in this study are available from the lead contact with a completed Material Transfer Agreement.

Data and code availability

- All data reported in this paper will be shared by the lead contact upon request.
- This paper does not report original code.
- Any additional information required to reanalyze the data reported in this work paper is available from the lead contact upon request.

EXPERIMENTAL MODEL AND STUDY PARTICIPANT DETAILS

Ethical issues

All experiments were conducted in compliance with the ARRIVE guidelines.

Animals

All experiments were performed in strict conformity with the European Union legislation for animal experimentation (European Committee Council Directive 2010/63/EU) and approved by the "Charles Darwin" Ethical Committee (authorization #6345–2016080822399698; committee Darwin CEEA #5). Mice were housed up to five per cage under standard conditions (12:12 h light-dark cycle; lights on at 7:00 a.m. and off at 7:00 p.m. referred to as zeitgeber time ZT0 and ZT12, respectively; 22 ± 2°C ambient temperature; 60% relative humidity) with food and water available *ad libitum*.

Mice were 8–20 weeks old, males, and weighted 23–30 g at the beginning of the experiments. Mice carrying two copies of the floxed allele of the exon 2 of *Slc17a8* (VGLUT3$^{lox/lox}$, RRID: IMSR_EM:05733; C57BL/6N background) were produced as previously described.[49] A knock-in mouse line expressing the Cre recombinase in VGLUT3 expressing neurons was generated at Cyagen (Santa Clara, CA) and was thereafter named VGLUT3^{Cre}. An internal ribosome entry site IRES-Cre cassette was placed downstream of the TAA stop codon of *Slc17a8* allowing Cre gene expression to be under the control of *Slc17a8* regulatory sequences in C57BL/6J mice. We additionally used heterozygous mice expressing the Cre recombinase only in neurons producing the 5-HT transporter (SERT^{Cre} mice[100]), the vesicular inhibitory amino acid transporter (VIAAT^{Cre} mice, strain #016962; The Jackson Laboratory, Bar Harbor, ME), or

the choline acetyltransferase (ChAT^{Cre} mice, strain #006410; The Jackson Laboratory). R26-stop-EYFP (Enhanced Yellow Fluorescent Protein) reporter line was obtained from The Jackson Laboratory (strain #006148). Adult male Swiss CD1 mice (12-20 weeks-old, body weight: 30–35 g) were obtained from Janvier Labs (Le Genest St. Isle, France). Genotypes of mice were determined by Polymerase Chain Reaction and electrophoresis before and after the end of the protocol.

Viral vectors

The following Adeno-Associated Viruses (AAVs) were produced by the Viral Vector Facility of the Neuroscience Center Zurich (Zentrum für Neurowissenschaften Zürich, ZurichSwitzerland): AAV-2/2-hSyn1-dlox-hM3D(Gq)-mCherry(rev)-dlox-WPRE-hGHp [AAV-DIO-hM3D(Gq)-mCh; 2.0e12 genome copies per mL (GC/mL)], AAV-2/2-hSyn1-dlox-mCherry(rev)-dlox-WPRE-hGHp (AAV-DIO-mCh; 5.6e12 GC/ml) and ssAAV-retro/2-hSyn1-dlox-EGFP(rev)-dlox-WPRE-hGHp(A) [rAAV-dlox-GFP; 4.5e12 genome copies per mL (GC/mL)]. The following AAVs: AAV2/1.CMV.HI.eGFP-Cre.WPRE (AAV-Cre-eGFP; 0.06–1.18e13 GC/ml), AAV2/1.CMV.PI.eGFP.WPRE.bGH (AAV-eGFP; 0.22–4.36e13 GC/ml), and AAV2/1.CAG.Flex.tdTomato.WPRE.bGH (AAV-Flex-tdTomato; 8.52e12 GC/ml) were obtained from Penn Vector Core (Philadelphia, PA) and were made available by Dr. Hongkui Zeng of the Allen Institute for Brain Science (Seattle, WA).

METHOD DETAILS

Experimental design

To delete VGLUT3 in the DR of adult mice, a virus expressing the Cre recombinase (AAV-Cre-eGFP) was infused in the DR of VGLUT3$^{lox/lox}$ mice. An AAV expressing the enhanced green fluorescent protein (AAV-eGFP) was used for control condition.

Conditional knock-out mice lacking VGLUT3 in 5-HT, GABAergic or cholinergic neurons were obtained by crossing VGLUT3$^{lox/lox}$ female mice to SERT^{cre}, VIAAT^{Cre}, or ChAT^{Cre} male mice, respectively. Mutant SERT$^{cre/+}$VGLUT3$^{lox/lox}$ (named SERT$^{VGLUT3.cKO}$), VIAAT$^{cre/+}$VGLUT3$^{lox/lox}$ (named VIAAT$^{VGLUT3.cKO}$) and ChAT$^{cre/+}$VGLUT3$^{lox/lox}$ (named ChAT$^{VGLUT3.cKO}$) mice were compared with VGLUT3$^{lox/lox}$ and SERT^{Cre}, VIAAT^{Cre}, or ChAT^{Cre} littermates, respectively.

A virus enabling conditional expression of the excitatory hM3 DREADD (Designer receptors exclusively activated by Designer Drugs[101]) receptor [AAV-DIO-hM3D(Gq)-mCh] was infused in the DR of VGLUT3^{Cre}, SERT^{Cre} and SERT$^{VGLUT3.cKO}$ mice to chemogenetically activate DR^{VGLUT3} neurons, and DR^{5-HT} neurons expressing VGLUT3 or not, respectively. Control non-DREADD-expressing mice were obtained by injecting an AAV enabling conditional expression of the fluorescent protein mCherry (AAV-DIO-mCh).

To map the targets of DR^{VGLUT3} neurons, a virus that enables conditional expression of the fluorescent protein tdTomato (AAV-Flex-tdTomato) was infused in the DR of VGLUT3^{Cre} mice.

To identify DR^{VGLUT3} neurons projecting to the ventral tegmental area (VTA), a retrograde virus that enables conditional expression of the fluorescent protein GFP (rAAV-dlox-GFP) was infused in the VTA of VGLUT3^{Cre} mice.

To identify VGLUT3 expressing neurons, conditional expression of the fluorescent protein EYFP in VGLUT3 expressing neurons was enabled by crossing VGLUT3^{Cre} male mice with ROSA26-stop-EYFP reporter female mice.[102]

Stereotaxic AAV injection

Mice were anesthetized with a mix of ketamine/xylazine [100 and 10 mg/kg, respectively, intraperitoneal (i.p.) injection] and fixed on a stereotaxic apparatus. Coordinates were adapted from the mouse brain atlas.[43] For conditional deletion of VGLUT3 and DREADD experiments, a dual injection of AAVs was done to target the whole DR [800 nL; from bregma, in mm: −4.8 (500 nL) and −4.3 (300 nL) anteroposterior, +0.9 lateral to the midline, −2.8 ventral from brain surface, 15° angle]. To map projections from DR^{VGLUT3} neurons, a single AAV injection was performed (200-500nL; from bregma, in mm: −4.5 anteroposterior, +0.9 lateral to the midline, −2.8 ventral from brain surface, 15° angle). To map DR^{VGLUT3} neurons projecting to the VTA, a bilateral AAV injection was performed (300 nL; from bregma, in mm: −3.1 anteroposterior, +0.5 and −0.5 lateral to the midline, −4.1 ventral from brain surface). A 10 μL Hamilton syringe with a microinjection needle was used to infuse AAVs at a rate of 100 nL/min. The needle was kept at the injection site for 5 min before removal. Mice were allowed to recover at least 3 weeks for tracing experiments prior to perfusion.

EEG and EMG surgical procedures

After removal of the microinjection needle used for AAV infusion, mice were instrumented for polygraphic sleep monitoring. Implantation of electrodes (enameled nichrome wires, 150 μm in diameter) was performed as described previously.[2] Briefly, two EEG electrodes were placed onto the dura over the right parietal cortex (from bregma, 2 mm caudal and 2 mm lateral to midline) and the cerebellum (from bregma, 5 mm caudal and at midline), two electrooculogram (EOG) electrodes were located subcutaneously on each side of the orbit and two electromyogram (EMG) electrodes were inserted into the neck muscles. All electrodes were soldered to a miniconnector (Antelec, La Queue en Brie, France) and anchored to the skull with dental acrylic. Polysomnographic recordings were performed at least 3 weeks later for DREADD experiments and 6 weeks later for conditional deletion of VGLUT3 in the DR.

Pharmacogenetic manipulation

Mice were habituated to manipulation and i.p. injections (7 days). Clozapine-N-oxyde (CNO) was injected i.p. at the dose of 1 mg/kg (Tocris Bioscience, Bio-Techne, Minneapolis, MN; catalog # 4936). CNO was suspended in a minimal volume of DMSO

(Sigma-Aldrich, St. Louis, MO) and saline (0.9%) was added to achieve a final 0.25% (v/v) DMSO in saline solution. There was at least a 2-day washout period between two CNO injections. To control for off targets effects of CNO, we included CNO-injected non-DREADD-expressing control mice, i.e., mice injected with the AAV-DIO-mCh.

Stress protocols

Acute social defeat stress (SD) was performed by placing an experimental mouse in a cage containing an aggressive resident male CD1 mouse for 5 min of physical defeat. Then, mice remained in the same cage but were physically separated by a perforated divider for the next 20 min, enabling sensory but not physical contact. The SD session started at 09:30 a.m. and lasted 25 min. The protocol was adapted from Challis et al. (2013).[24] Aggressive CD1 male mice were selected according to published methods[98] and kept in large cages (19 × 35 × 14 cm^3) for the rest of the experiment. Acute restraint stress (RS) was performed by wrapping each mouse in a nylon-covered metal mesh for 90 min, from 5:30 to 7:00 p.m., as previously described.[1]

Sleep/wake monitoring

Mice were placed in individual recording chambers [custom-made Plexiglas cages (19 × 19 × 30 cm^3)] and connected to the recording system with a light-weight cable and a swivel enabling free movements. Mice were acclimated to the recording conditions for 4 days before starting the recordings.

Baseline sleep recordings were performed for 24 h starting at dark onset (7:00 p.m.). To assess the impact of stress on sleep, mice were placed back into their home cage after RS or SD, connected back to the recording cables, and immediately recorded. Each mouse was used as its own control. In the SD protocol, matched control recordings were obtained from baseline sleep recordings. In the RS protocol, matched control recordings (sham condition) were obtained one or two days prior to the stress session: mice were woken up at the two time-points corresponding to the beginning and the end of stress procedure (5:30 p.m. and 7:00 p.m.). The two stress sessions were performed at least one week apart. For DREADD experiments, mice were injected at 10:00 a.m. with saline (control matched recording) or CNO (1 mg/kg) and recorded for 21 h.

Infrared thermography

Thermal imaging was performed in single-housed mice following CNO injection (1 mg/kg at 10:00 a.m.), SD (25 min session ending at 10:00 a.m.) or RS (90 min session ending at 7:00 p.m.). Matched control thermal images were obtained just before the stress session. Skin temperature at the lumbar back and at the level of the intrascapular brown adipose tissue (BAT) were imaged with an infrared camera (B335: Compact-Infrared-Thermal-Imaging-Camera; FLIR; West Malling, Kent, UK) and analyzed with an FLIR-Tools Software (FLIR; West Malling). For each image, the area at the most caudal part of the back or the area of the intrascapular BAT was delimited, in which the maximal temperature was selected. For each mouse and experimental condition, the maximal temperature is the average of five images.

Behavioral tests

Mice were placed in the experimental room at least 45 min before the beginning of the tests. The tests were performed between ZT2 and ZT6. For chemogenetic experiments, mice were injected with CNO (1 mg/kg) and tested 30 min later.

Locomotor activity

Locomotor activity was tested in an open filed. The open field test was performed in a white Perspex arena (43 × 43 × 26 cm^3) with 40 lux intensity light in the center. The virtual central zone measured 20 x 20 cm^2. Mice were introduced into one corner of the arena and allowed to freely explore the open field for 600 s. The distance traveled in the arena was evaluated by video tracking (Ethovision XT 14.0, Noldus, Wageningen, Netherlands) as an index of locomotor activity.

Anxiety-like behavior

The light/dark box test was performed in a two compartmented arena. One compartment is a black closed chamber deprived of light (15 × 21 × 21 cm^3) and the other is white exposed to a 120 lux intensity light (30 × 21 × 21 cm^3, anxiogenic zone) linked by a rectangular opening (7 × 5 cm^2). Mice were introduced into the dark compartment and allowed to freely explore the arena for 360 s. The time, and distance traveled in the light zone were evaluated by video tracking (Ethovision XT 14.0) as an index of an anxiety-related response.

Anatomical validation of AAV injections

After experiments, histological analysis was performed to control for location of AAV injection and expression. Mice that did not show viral expression (tdTomato, mCherry or eGFP fluorescence) or proper targeting were not included in subsequent data analysis. In addition, Cre-driven recombination of the floxed exon 2 of *Slc17a8* was validated using *in situ* hybridization (ISH).

In situ hybridization (ISH)

To estimate the proportion of 5-HT neurons expressing VGLUT3 in the mouse anterior raphe nuclei, we used a digoxigenin (DIG)-labeled probe directed against VGLUT3 mRNA (*Slc17a8;* GenBank: NM_182959.3; corresponding to nucleotides 1899–2320) and a fluorescein-labeled probe to detect the mRNA encoding TPH2 (tryptophan hydroxylase type 2; GenBank: NM_173391.3; corresponding to nucleotides 270–1262), a marker of 5-HT neurons.

To control that Cre expression is restricted to VGLUT3 expressing neurons in VGLUT3^{Cre} mice, we used a DIG-labeled probe directed against the Cre recombinase (GenBank: AB_449974.1; corresponding to nucleotides 245–1060) and a fluorescein-labeled probe to detect the mRNA encoding VGLUT3.

To validate reduced VGLUT3 expression mediated by AAV-Cre injection in the DR, we used a DIG-labeled Probe (Probe 1, corresponding to nucleotides 425–595) for detection of exon 2. Probe 1 identifies cells expressing the wild-type VGLUT3 mRNA while recombined cells lack Probe 1 labeling. We additionally labeled TPH2 mRNA by using a fluorescein-labeled probe (see above).

To validate SERT$^{VGLUT3.cKO}$ mice, a two-probe approach was implemented to identify cells expressing the VGLUT3 mRNA missing exon 2 generated by the Cre-driven recombination of the floxed *Slc17a8*. DIG-labeled Probe 1 (corresponding to nucleotides 425–595) was designed for detection of exon 2 and fluorescein-labeled Probe 2 (corresponding to nucleotides 1899–2320) for detection of exon 12 of VGLUT3 mRNA, respectively. Recombined cells can thus be identified based on lack of Probe 1 labeling and presence of probe 2 labeling as previously described for the gene encoding the vesicular monoamine transporter 2.[103] To further assess whether recombination occurs in 5-HT neurons, we additionally labeled TPH2 mRNA by using a fluorescein-labeled probe (see above).

Mice were euthanized and brains were quickly removed, frozen in isopentane chilled at −30°C and stored at −20°C. The frozen brains were cut into three series of 14-μm-thick coronal sections at the level of the DR using a cryostat (CM3050S; Leica Microsystems, Wetzlar, Germany) and thaw-mounted onto poly-*l*-lysine-coated glass slides (Superfrost Plus, Menzel Glaser, Braunschweig, Germany). The collected sections were stored at −80°C before being processed for ISH labeling.

Dual fluorescent ISH (FISH) was performed as described previously.[104] Briefly, complementary RNA probes were synthesized with DIG- or fluorescein-labeled ribonucleoside tri-phosphate (Sigma-Aldrich). The specificity of the probes was verified using NCBI blast. Cryosections were air-dried, fixed in 4% paraformaldehyde and acetylated in 0.25% acetic anhydride/100 mM triethanolamine (pH = 8). Sections were hybridized for 18 h at 65°C in 100 μL of formamide-buffer containing 1 μg/mL DIG-labeled riboprobe and 1 μg/mL fluorescein-labeled riboprobe. Sections were washed at 65°C with SSC buffers of decreasing strength, and blocked with 20% fetal bovine serum (Thermo Fisher Scientific, Waltham, MA) and 1% blocking solution (Sigma-Aldrich). Fluorescein epitopes were detected with horseradish peroxidase (HRP) conjugated anti-fluorescein antibody at 1:5000 (Roche, Mannheim, Germany; Cat# 11426346910, RRID: AB_840257) and revealed using Cy2-tyramide at 1:250. HRP-activity was stopped by incubation of sections in 0.1 M glycine followed by a 3% H2O2 treatment. DIG epitopes were detected with HRP anti-DIG Fab fragments at 1:3000 (Roche, Mannheim, Germany; Cat# 11207733910, RRID: AB_514500) and revealed using Cy3 tyramide at 1:100. At the end of these procedures, sections were coverslipped with Fluoromount-G mounting medium (Southern Biotech, Birmingham, AL) and stored in the dark at 4°C before microscopy and imaging. For combined FISH and brightfield ISH, the protocol was the same as described above until revelation as described previously.[105] Briefly, fluorescein epitopes were detected with HRP conjugated anti-fluorescein antibody at 1:5000 and revealed using Cy2 tyramide at 1:250. DIG epitopes were detected with alkaline phosphatase conjugated anti-Dig antibody at 1: 1000 (Roche, Mannheim, Germany. Cat# 11093274910, RRID: AB_514497) and signal developed with NBT/BCIP (*p*-nitroblue tetrazolium chloride/5-bromo-4-chloro-3-indolyl phosphate; 1/100).

Immunohistochemistry (IHC)

To identify whether VGLUT3 terminals originating from the DR display a mixed glutamate/5-HT phenotype, we performed 5-HT immunolabeling in VGLUT3^{Cre} mice injected with an AAV-Flex-tdTomato in the DR.

To study the effects of chemogenetic activation of DR^{VGLUT3} neurons, mice were injected with CNO (1 mg/kg) and perfused 90 min later. Brains were processed for c-Fos immunolabeling.

To assess stress-induced c-Fos expression in DR^{VGLUT3} neurons, VGLUT3^{EYFP} male mice were perfused at the end of the 90-min RS or 1 h after the 25-min SD. Brains were processed for triple Fos/EYFP/TPH2 immunolabeling. To assess stress-induced c-Fos expression in DR^{VGLUT3} neurons projecting to the VTA, VGLUT3^{Cre} male mice injected with a rAAV-dlox-GFP in the VTA were perfused 1 h after the 25-min SD. Brains were processed for triple c-Fos/GFP/TPH2 immunolabeling. Control groups consist of unstressed mice left in their home cage and briefly manipulated before being perfused 90 min later.

Mice were sedated with sodium pentobarbital (80 mg/kg, i.p.) and perfused intracardially with 50 mL of 4% paraformaldehyde (PFA) in PBS (50 mM NaH2PO4/Na2HPO4 and 154 mM NaCl, pH 7.4). The brains were removed and post-fixed overnight. Then, three series of 35 μm-thick coronal brain sections were cut using a vibratome (VT-1000, Leica Microsystems, Wetzlar, Germany), and stored in PBS-azide (0.02%) solution at 4°C before use.

Brain sections were incubated at 4°C for 48 h with primary antibodies in PBS containing 0.3% Triton X-100 (Sigma Aldrich) and 4% normal horse serum (Thermo Fisher Scientific). 5-HT was detected with a rabbit polyclonal anti-5-HT (1:5000; Sigma-Aldrich; #S5545, Lot #075K4779; RRID: AB_477522). A rabbit polyclonal anti-*c*-Fos antiserum was used to detect c-Fos (1:2000; Abcam, Cambridge, UK; #190289, Lot #GR3244475-2 and #GR1065369-1, RRID: AB_2737414). EYFP and GFP were detected with a chicken polyclonal anti-GFP (1:2000; Aves Labs, Portland, OR, USA; #1020, Lot #3717982; RRID: AB_10000240). TPH2 was detected with a mouse monoclonal anti-TPH2 (1:1000; Sigma-Aldrich; #T0678, Lot #064M4815V; RRID: AB_261587 or Abcam; #211528-1001, Lot #GR3344910-18).

For single c-Fos immunolabeling, sections were then rinsed in PBS supplemented with 0.1% Triton X-100 and incubated for 2 h with biotinylated anti-rabbit IgG (1:200 dilution; Vector Laboratories, Burlingame, CA, USA; #PI-1000, RRID: AB_2313606) in PBS containing 4% BSA and 0.1% Triton X-100. Additional rinses were followed by incubation with avidin-biotin-horseradish peroxidase solution (ABC Vectastain Elite kit; Vector Laboratories) for 1 h, and c-Fos immunoreactivity was visualized as a brown reaction

product after incubation of the sections with 0.04% (w/v) of 3,3′-diaminobenzidine (DAB; Sigma-Aldrich) in PBS, supplemented with increasing concentrations of H_2O_2 (from 0.00015 to 0.0048%). Stained sections were mounted on poly-/-lysine-coated glass slides, dehydrated, and coverslipped with Eukitt mounting medium (Thermo Fisher Scientific).

For dual c-Fos/EYFP or c-Fos/GFP immunolabeling, sections were rinsed after incubation with primary antibodies in PBS and incubated for 1 h with anti-rabbit IgG coupled to Alexa Fluor 594 (1/1000; Thermo Fisher Scientific; Cat# A-21207; RRID: AB_141637), and anti-chicken IgY coupled to Alexa Fluor 488 (1:1000; Thermo Fisher Scientific; Cat# A32931, RRID: AB_2762843). For triple c-Fos/EYFP/TPH2 or Fos/GFP/TPH2 immunolabeling, sections were rinsed after incubation with primary antibodies in PBS and incubated for 1 h with anti-rabbit IgG coupled to Alexa Fluor 594 (1/1000; Thermo Fisher Scientific; Cat# A-21207; RRID: AB_141637), anti-chicken IgY coupled to Alexa Fluor 488 (1:1000; Thermo Fisher Scientific; Cat# A32931, RRID: AB_2762843) and anti-mouse IgG coupled to abberior STAR 635P (1/1000, Abberior GmbH, Göttingen, Germany; Cat# ST635-1001).

After rinses, sections were coverslipped with Fluoromount-G mounting medium (Thermo Fisher Scientific) and stored in the dark at 4°C before microscopy and imaging.

Nomenclature and abbreviations

The nomenclature used to describe the raphe nuclei was adopted, for the most part, from subsequent reports in the mouse brain.[16,106] We distinguished the B9 group and 5-HT neurons in the interpeduncular complex (IP), the median raphe nucleus (MnR, that includes the B8 and B5 cell groups), the dorsal raphe nucleus (DR; B7 [rostral part] and DRc; B6 [caudal part] groups). The DR was further subdivided into the ventral (DRv) part, the lateral (DRl) part and the dorsal part (DRd).

Other abbreviations used include anterior commissure (aca); aqueduct (aq); basal forebrain (BF); basolateral amygdala (BLA); diagonal band nucleus (NDB); fourth ventricle (4V); locus coeruleus (LC); magnocellular nucleus (MA); medial forebrain bundle (mfb); mesencephalic trigeminal nucleus (me5); nucleus accumbens (NAc); parabrachial region (PB); external lateral parabrachial subnucleus (PBel); prelimbic cortex (PL); superior cerebellar peduncle (scp); tryptophan hydroxylase type 2 (TPH2); ventral tegmental area (VTA); vesicular glutamate transporter type 3 (VGLUT3).

QUANTIFICATION AND STATISTICAL ANALYSIS

Sleep analysis

EMG and EEG signals were recorded with Somnologica software (Medcare, Reykjavik, Iceland), amplified, analog-to-digital converted (2 kHz) and down-sampled at 100 Hz (EMG) or 200 Hz (EEG), and digitalized by an AddLife A/D Module. Polygraphic sleep recordings were visually scored offline every 10 s as wake (W), non-REMS (NREMS) and REMS following classical criteria using the Somnologica software (Medcare). Vigilance states amounts for each animal were expressed as minutes per 3 h, 6 h or 12 h intervals. The sleep architecture was assessed by calculating the mean duration and frequency of vigilance states bouts (a bout could be as short as one epoch).

Image acquisition and processing

For FISH and tracing experiments and single c-Fos labeling, slides were scanned on a NanoZoomer 2.0-HT (Hamamatsu Photonics, Shizuoka, Japan) at 20× resolution. Laser intensity and time of acquisition were set separately for each labeling. Image microphotographs were analyzed using the NDP2.view software (Hamamatsu Photonics). For dual/triple fluorescent immunolabeling, images were acquired using confocal laser scanning microscope (Leica TCS SP5 with LCS Leica software). For illustration purposes, the images were exported in TIFF format and were then corrected for contrast, cropped and assembled on Photoshop CS2 (version 9.0; Adobe Systems, Mountain View, CA, USA). Finally, additional indications and/or anatomical landmarks were incorporated.

Quantification of labeling

Dual FISH was imaged using the NanoZoomer 2.0-HT. All single VGLUT3-, TPH2-, and double VGLUT3/TPH2-mRNA labeled neurons in the different raphe nuclei were counted in 2–6 different brain sections, 85 μm apart, without considering the intensity of the staining. For each mouse, the number of labeled cells of each type was then averaged.

Single c-Fos immunolabeling was imaged using the NanoZoomer 2.0-HT. Brain regions of interest were delineated using the mouse brain atlas.[43] For each region, c-Fos positive cells were counted in 2–4 sections per mouse, 105 μm apart, without considering the intensity of the signal. For each mouse, the number of labeled cells for a given structure was then averaged.

Fluorescent immunolabeling was imaged using a confocal laser scanning microscope (Leica TCS SP5 with LCS Leica software). Cell counts were performed using the Fiji ImageJ software and QuPath v0.5. For dual labeling, all single EYFP and double EYFP/c-Fos labeled neurons in the DR were counted in two different brain sections, 105 μm apart, at 2 different Z-stacks without considering the intensity of the staining. For triple labeling, all single EYFP (or GFP), double EYFP (or GFP)/c-Fos labeled neurons TPH2 immunonegative (TPH2-) and triple EYFP (or GFP)/c-Fos TPH2 immunopositive (TPH2+) labeled neurons in the DR were counted in two different brain sections, 105 μm apart, at 2 different Z-stacks without considering the intensity of the staining. Neurons expressing VGLUT3 were identified by the presence of an EYFP/GFP signal visible within both the soma and nuclei of neurons. VGLUT3/TPH2-positive neurons were identified by the presence of overlapping EYFP/GFP and TPH2 signals. VGLUT3/c-Fos positive neurons exhibited a confined c-Fos signal within the nucleus of neurons displaying EYFP/GFP signal. VGLUT3/c-Fos/TPH2+ neurons exhibited a confined c-Fos

signal within the nucleus of neurons exhibiting overlapping EYFP/GFP and TPH2 signals within the soma. For each mouse, the number of labeled cells of each type was then averaged.

To control for Cre-LoxP-mediated deletion of *Slc17a8* mediated by AAV-Cre injection in the DR of VGLUT3$^{lox/lox}$ mice, single VGLUT3 mRNA labeling in the raphe nuclei was assessed in 5 different brain sections, 85 μm apart. Quantifications of VGLUT3-positive signal were performed using ImageJ software, taking into account the cells with immunofluorescence above a threshold chosen to obtain optimal signal-to-noise ratio. Intensity of the staining was then evaluated after background subtraction. For each mouse, total VGLUT3 amounts were assessed in the DR and the MnR. Results are presented as normalized over the averaged total VGLUT3 amounts of control mice (-Cre).

Statistics

Data are presented as mean ± SEM. All data were analyzed using Prism 9.0 (GraphPad, San Diego, CA, USA). Normality assumptions were first verified prior to the use of any parametric tests (D'Agostino & Pearson normality test or Shapiro-Wilk normality test). In case of violation of normality assumption, non-parametric tests were used or data were log transform. We performed two-way analysis of variance (ANOVA) and repeated measure two-way analysis of variance (RM ANOVA). If significant effects were observed, post-hoc t-tests with Bonferroni corrections for multiple comparisons were performed. We also performed one-way ANOVA or Mann-Whitney test to compare group means. Statistical analyses are described in Table S6. Data were considered to be statistically significant when $p < 0.05$. All tests were performed on raw data.